buildings

MDPI

Article

Attitude Control Criteria for Non-Closed Segmental Lining Rings and Bolts Under Asymmetric Loading

Zihan Zeng [1], Junyi Zhang [1], Fanghui Pan [2,*], Jun Liu [3], Haolin Huan [3], Yan Qiu [4], Xiaoyong Kou [4] and Changhong Wang [5]

[1] College of Environmental Science and Engineering, Donghua University, Shanghai 201620, China; zzhzzhzzh1218@163.com (Z.Z.); 13788977592@163.com (J.Z.)
[2] Water Resources and Water Environment Engineering Technology Center, Xinjiang Key Laboratory of Synthesis and Application of Carbon Nanomaterials, School of Civil Engineering, Kashi University, Kashi 844000, China
[3] College of Urban Railway Transportation, Shanghai University of Engineering Science, Shanghai 201620, China
[4] Shanghai Tunnel Engineering Co., Ltd., Shanghai 200032, China
[5] Department of Civil Engineering, Shanghai University, Shanghai 200444, China
* Correspondence: pfh20072008@126.com

Abstract

Synchronous Thrust and Assembly Technology (STAT), which enables simultaneous shield propulsion and segment erection, can improve tunneling efficiency and reduce construction duration compared with conventional shield tunneling. However, during STAT construction, thrust from shield tail jacks directly acts on incomplete segmental lining rings before ring closure. Differential jack strokes caused by shield attitude fluctuations and segment assembly errors may therefore induce localized asymmetric stress distributions, resulting in segment deflection, joint misalignment, and potential structural damage. To evaluate these risks, this study develops a case-based methodological framework for assessing the mechanical safety of incomplete segmental lining rings and bolts under asymmetric loading conditions, using the Shanghai Rail Transit Airport Link Line tunnel as the engineering case. A refined finite element model was established to analyze the critical deflection behavior of incomplete segmental lining rings subjected to jack thrust during assembly. Field tests were conducted to monitor bolt mechanical responses under STAT conditions and to provide engineering validation for the numerical results. In addition, the critical differential jack stroke was determined based on the shield machine's maximum design turning radius and shield tail clearance. Within the modeled one- to three-segment assembly stages, the inter-segment restraint progressively increased, reducing segment deformation and bolt loads. No saturation of the clamping effect beyond the third segment was claimed. The simulated maximum segment deflection angle corresponds to a differential jack stroke below the shield kinematic limit of 21.9 cm. To maintain the mechanical safety of incomplete segmental lining rings within the investigated project conditions, the segment deflection angle should be controlled below the minimum damage initiation angle of 0.4°. The numerical model evaluated bolt responses during the single-segment stage; however, field measurements were available only after the second segment installation and therefore did not directly validate the most unfavorable single-segment stage. By integrating segment damage thresholds, bolt stress responses, shield tail clearance, and jack stroke constraints, project-specific attitude deviation control criteria were proposed for the investigated large-bore shield-driven tunnel. It should be noted that these criteria were derived from a specific finite element model and limited field measurements from one engineering case; therefore, recalibration and further validation are required before applying the proposed thresholds to shield tunnels with different diameters, segment geometries, geological conditions, or shield machine configurations.

Check for updates

Academic Editor: Eugeniusz Koda

Received: 30 May 2026
Revised: 1 September 2026
Accepted: 24 September 2026
Published: 29 October 2026

Copyright: © 2026 by the authors. Licensee MDPI, Basel, Switzerland. This article is an open access article distributed under the terms and conditions of the Creative Commons Attribution (CC BY) license.

Keywords: large-bore shield-driven tunneling; simultaneous propulsion and segment erection; attitude control criteria; incomplete segmental lining rings; asymmetric stress distribution

1. Introduction

Currently, the construction of large-diameter shield tunnels has become a critical component of urban underground transportation infrastructure, significantly alleviating traffic congestion, preserving ecological environments, and enhancing land-use efficiency [1,2]. During tunnel construction, both construction speed and quality are pivotal factors constraining the development of transportation systems [3]. Beyond construction efficiency, the resilience and safety of shield tunnel systems under uncertain ground and environmental conditions have also attracted increasing attention. Recent studies have emphasized that the spatial variability in soil properties introduces substantial uncertainty into the seismic response of soil–shield tunnel systems, highlighting the importance of considering geological uncertainty in tunnel safety and resilience assessment [4]. These requirements drive the need for faster tunneling, which can be achieved by simultaneously performing shield thrust and segment assembly—a technique that uses Synchronous Thrust and Assembly Technology (STAT).

Large-diameter shield tunneling presents numerous challenges, including lower advance rates and increased segment quantities. The time allocated to thrust propulsion and segment assembly directly impacts overall construction progress. As an innovative alternative, synchronous thrust–assembly technology has evolved internationally since the 1990s with several novel methodologies. (1) Lose-Zero Method [5]: This technique utilizes redundant cylinder strokes generated during the axial insertion of the key segment for segment assembly, enabling partial synchronization while maintaining thrust continuity. (2) F-Navi Method: A spherical oscillating mechanism installed in the shield machine's front section enables real-time attitude control, achieving concurrent tunneling and segment assembly with linear alignment accuracy. (3) Lattice-Type Cylinder Shield Method: Employing a double-shield configuration with lattice-arranged cylinders, this method controls cutterhead attitude through telescopic motion while providing reverse torque capacities. The front shield's telescoping functionality allows for continuous thrust during segment assembly. (4) Dual-Cylinder Synchronous Thrust and Assembly Technology Method: This method features a sliding inner cylinder equipped with forward-extending thrust cylinders and rear-extending assembly cylinders. For the final method, the sliding-inner-cylinder configuration enables simultaneous thrust force application and segment installation within the inner cylinder's reaction zone. Domestic research on STAT remains in its nascent stage, with limited engineering applications. A full-scale experimental platform was deployed to simulate linear single-ring construction processes, evaluating thrust force control accuracy, tunneling speed optimization, shield attitude maintenance and segment compression integrity [6]. The results confirmed the feasibility and reliability of synchronous methods under controlled asymmetric loads, providing critical references for large-diameter tunnel applications.

In conventional shield tunneling, hydraulic jacks must wait until segment rings are fully closed to propel the shield machine by pushing against completed lining rings. Although existing shield attitude control methods have been widely used in conventional shield tunneling, they are not sufficient for STAT operations. Current control approaches mainly focus on geometric indicators, such as shield axis deviation, shield tail clearance, jack stroke difference, and real-time attitude correction. These methods are effective for maintaining shield alignment when the thrust system acts on completed and closed lining

rings. However, under STAT conditions, newly erected segments are incomplete and lack full circumferential constraints, while shield jack thrust is directly applied to the unclosed segmental lining rings. As a result, the load transfer path, segment–bolt interaction, and damage evolution mechanism differ substantially from those in conventional tunneling. Existing attitude control methods generally do not establish a quantitative relationship between shield attitude deviation, differential jack strokes, segment damage thresholds, and bolt stress safety. Therefore, they cannot directly determine whether a given shield attitude deviation is mechanically safe for incomplete segmental lining rings during synchronous propulsion and segment erection. To address this gap, this study develops a coupled segment–bolt mechanical analysis framework and converts critical segment deflection angles into allowable differential jack strokes, thereby providing a quantitative basis for project-specific attitude control criteria under STAT conditions. In contrast, STAT integrates segment assembly with shield advancement, thereby reducing downtime caused by sequential operations [7,8]. However, misalignment between segments during construction often induces structural damage and adversely affects connecting bolts. Such issues compromise tunnel safety, durability, and long-term maintenance costs [9]. Shield tail clearance provides critical guidance for shield machine attitude adjustment and segment selection during tunneling. Machine vision-based methods enable the precise determination of segment axis positions, achieving the real-time measurement of shield tail clearance during construction. A large-scale indoor model test platform for shield tunneling was developed to conduct shield attitude adjustment experiments, examining soil–structure interactions under both in situ attitude adjustment and tunneling attitude adjustment modes [10]. Defects introduced during segment assembly may propagate cumulative damage during subsequent construction phases, ultimately jeopardizing overall tunnel quality [11–13]. Additionally, a model of a large-diameter slurry shield traversing existing tunnels was established [14]. The solution for semi-infinite saturated soil was applied to deformation prediction, providing safety indices as a preliminary assessment tool for tunnel design. An analytical model for calculating the additional response of the segmental lining under asymmetric thrusts was established, where the performance was verified via convincing numerical simulations, and an in-depth sensitivity analysis was conducted to explore the effect of the critical parameters [15].

Research on segment damage primarily employs three methodologies: experimental or field measurement analysis [16], numerical analysis using the finite element method [17,18], and theoretical modeling [16]. Most studies integrate field data with the FEM to mutually validate findings and investigate damage mechanisms in shield tunnel segments. During assembly, inherent errors in segment erectors and segments themselves propagate static deviations to adjacent rings, making defect pattern analysis critical for ensuring assembly quality. A detailed numerical model of cast iron segment joints was developed and validated through full-scale tests, emphasizing crack initiation at key structural zones and joint behavior impacts [19]. A statistical analysis of segment damage causes categorizes assembly-induced defects into three morphological types [20]. A refined FEM model was established to analyze damage mechanisms under jack thrust forces, particularly addressing ring face unevenness and incomplete inter-segment contact. A mathematical model was subsequently proposed to quantify tolerance–contact defect relationships [21]. Recognizing the strong correlation between assembly imperfections and structural damage, Japanese engineers conducted a survey across 50 projects and 15 contractors, revealing longitudinal cracking and corner spalling as predominant failure modes.

The increasing number of tunnel segments introduces structural complexity due to inter-segment joints. Since bolts are embedded within segments and their stress states cannot be visually inspected, ensuring their mechanical safety has become a critical focus. Researchers have investigated bolt behavior through full-scale tests, numerical simulations,

and analytical models. Finite element joint models [22] were refined using local stiffness correction factors, revealing that joint influence zones are limited, and lining rings fail primarily due to segment rotation and localized compression. The interaction mechanisms of relative radial displacements between adjacent rings under localized loads were explored [23], demonstrating that longitudinal horizontal displacements significantly affect deformation patterns and internal force distributions. A beam-joint discontinuity model [24] was developed to analyze shield jack thrust and angular deviations, identifying these parameters as key factors influencing segment and circumferential bolt stresses. Existing studies have predominantly focused on the failure mechanisms of segments and bolts, analyzing these two components in isolation. However, under STAT conditions, the mechanical interactions between these structures differ significantly, necessitating a refined investigation into their combined stress states to ensure structural integrity and operational safety.

To provide an engineering basis for the proposed attitude control criteria, the Shanghai Rail Transit Airport Link Line (Western Section) was selected as the case project in this study. This project represents a practical large-bore shield-driven tunneling case in which the STAT method was applied during construction. It is not merely a background project but serves as the engineering source for determining shield machine parameters, segment geometry, construction procedures, numerical modeling conditions, and field test arrangements. Specifically, the shield machine configuration, segmental lining dimensions, and synchronous propulsion–segment erection process of this project were used to establish finite element models and define asymmetric loading scenarios. In addition, field measurements of bolt mechanical behavior were carried out on site to validate the numerical results and support the establishment of attitude control criteria. Therefore, the following project overview is introduced to clarify the engineering context, data source, and practical validation basis of the proposed methodology. With advancements in tunneling technology, significant differences exist between the internal structural forces of conventional shield methods and those under STAT [25,26]. Compared to traditional tunneling, newly assembled segments in STAT lack hoop effects on both sides, and unclosed segment rings directly bear jack thrust forces. Assembly errors under such conditions critically impact the ultimate load-bearing capacity of the segment–bolt system [27–29]. This study proposes a methodological framework to establish control criteria for mitigating asymmetric stress effects on segments and bolts during STAT, aiming to reduce damage risks. To address the mechanical safety issues of incomplete segmental lining rings and connecting bolts under STAT conditions, this study aims to establish a systematic attitude control framework for large-bore shield-driven tunneling subjected to asymmetric loading. The specific objectives are to clarify the stress redistribution and damage evolution mechanisms of incomplete segmental lining rings during simultaneous propulsion and segment erection, evaluate the mechanical response and safety state of circumferential and longitudinal bolts, and determine the allowable shield attitude deviation during construction. To achieve these objectives, refined finite element models are developed to simulate the load-bearing behavior of segmental linings under different asymmetric loading modes, including radial inward deflection, radial outward deflection, and lateral deflection. Field tests are further conducted to monitor bolt stress responses under STAT conditions and to verify the reliability of the numerical results. On this basis, the critical deflection angles of segments are converted into corresponding differential jack strokes according to the geometric relationship between shield attitude deviation and jack displacement. By integrating segment damage thresholds, bolt stress safety, shield tail clearance, and the maximum design turning radius of the shield machine, quantitative attitude control criteria are finally established to validate structural safety, guide segment erection, and provide construction control standards for large-diameter shield tunneling under STAT.

2. Case Project and Engineering Background

2.1. Description of Case Project

The Shanghai Rail Transit Airport Link Line (Western Section) is Shanghai's first regional railway line operating in a metro-style format. Spanning approximately 68.6 km with an east–west alignment, this project connects two major transportation hubs: Shanghai Hongqiao International Airport and Shanghai Pudong International Airport. It comprises nine stations and is divided into three segments, the Puxi Section, Pudong Section, and River-Crossing Section, with 56.7 km of underground tunnels. The entire line adopts a double-track railway system, utilizing multiple China Railway High-speed regional electric units with a maximum design speed of 160 km/h. Key shield tunneling sections include: Shield Tunnel TBM No. 1: Meifu Road Shaft → Piston Vent Shaft → Huajing Station (2148 m total). Shield Tunnel TBM No. 2: Meifu Road Shaft → Shaft No. 3 → Shaft No. 2 (5657 m total). The alignment and segment divisions are illustrated in Figure 1.

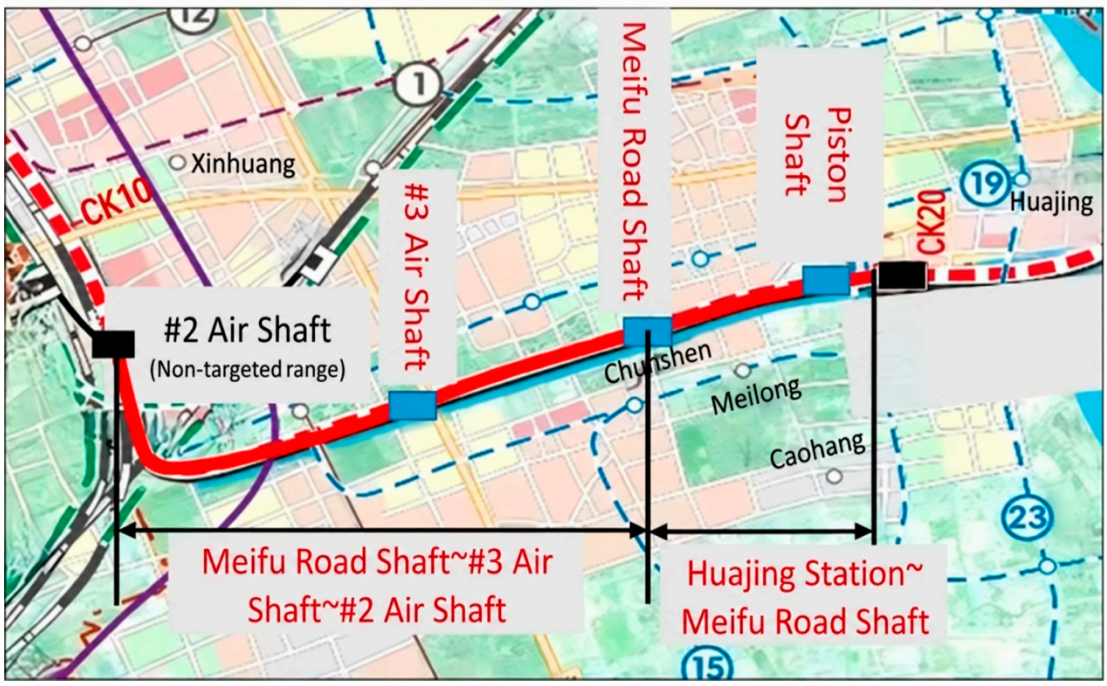


Figure 1. Schematic diagram of shield route.

2.2. Geological Condition

The tunnel primarily traverses three geological strata, Layer ⑤$_1$ silty clay, Layer ⑥$_1$ silty clay, and Layer ⑦$_1$ silty sand with clay interbeds, with detailed stratigraphic configurations illustrated in Figure 2. The alignment crosses a region with a well-developed surface water system, characterized by interconnected rivers and canals, including Chunshen Creek, Meilong Canal, and multiple unnamed waterways.

Preliminary geotechnical investigations reveal a complex groundwater regime comprising: phreatic water in shallow soils; semi-confined aquifers within Layer ④$_t$ silty sand, Layer ⑤$_{1t}$ silty sand–clay interbeds, Layer ⑤$_{32}$ silty sand–clay interbeds, and Layer ⑤$_{42}$ silty sand; and confined aquifers in Layers ⑦, ⑧$_2$, and ⑨. The hydraulic connectivity between surface water and groundwater systems poses significant challenges for attitude control during large-diameter shield tunneling in this hydrogeologically sensitive zone [30].

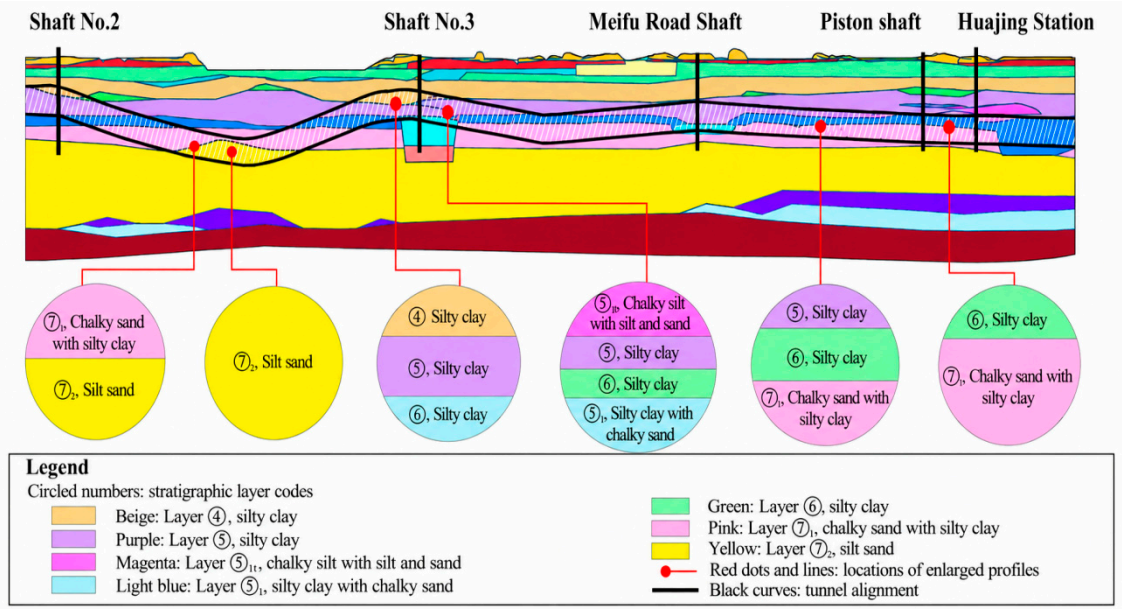


Figure 2. Longitudinal geological profile of the soil layers. Circled numbers denote the stratigraphic layer codes, and colors represent different soil types, as defined in the legend. Red dots and connecting lines indicate the locations of the enlarged geological profiles.

2.3. STAT Method and Mechanical Equipment

The large-diameter shield tunneling machine employed in this project was independently developed by Shanghai Tunnel Engineering Co., Ltd. (conceptual model shown in Figure 3). Key specifications include a shield diameter of 14.07 m, total weight of 3200 t, total length of 99 m (16 m main drive section), cutterhead diameter of 14.05 m, and maximum advance rate of 60 mm/min. To address the project's technical complexity, the STAT process adheres to a "uniform pressure per segment block" principle, enabling the real-time monitoring of hydraulic cylinder pressures and stroke variations. The operational sequence comprises three cyclic phases. First, thrust cylinders corresponding to the first segment retract while maintaining pressure continuity. Cylinder thrust transitions smoothly to the operational load case. Second, following first segment fixation, its corresponding cylinders extend while second segment cylinders retract. Thrust redistribution maintains equilibrium across active segments. Third, the process iterates until all three segments achieve full circumferential closure. During construction, the shield machine aids the transition of thrust system pressure control from a passive response in conventional thrust mode to active control in STAT mode through thrust cylinder pressure regulation, as illustrated in Figure 4. Jack retraction and thrust force configuration are automatically executed by the shield machine. Unlike traditional thrust methods, under STAT conditions, thrust forces are rationally allocated to unassembled segments, optimizing load distribution and minimizing asymmetric stress concentrations.

During the synchronous assembly–propulsion process, the shield machine attitude is controlled by adjusting the pressure distribution of the hydraulic cylinders (Figure 5). It can be observed that the thrust of the cylinders is not uniformly distributed along the circumferential direction; instead, it exhibits a certain degree of asymmetry depending on the attitude control requirements and segment erection conditions. Cylinders with higher loads are primarily concentrated in the direction of attitude correction, ensuring the alignment control of the tunneling axis and the precision of segment installation. Overall, this thrust distribution reflects the dynamic coordination and real-time regulation mechanism of the propulsion system under synchronous assembly–propulsion conditions.

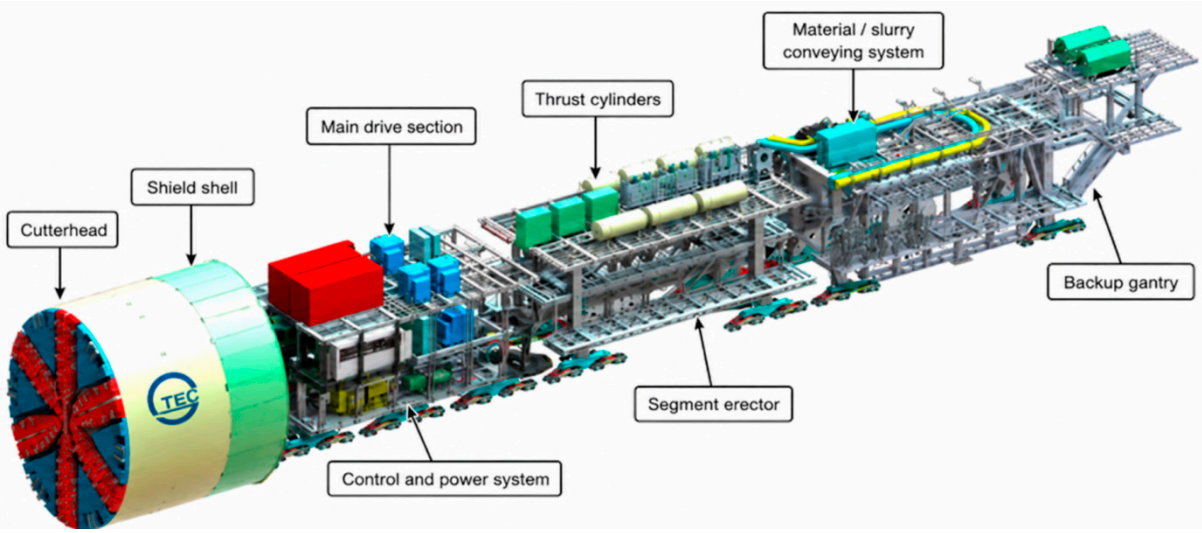


Figure 3. Schematic diagram of shield machine model.

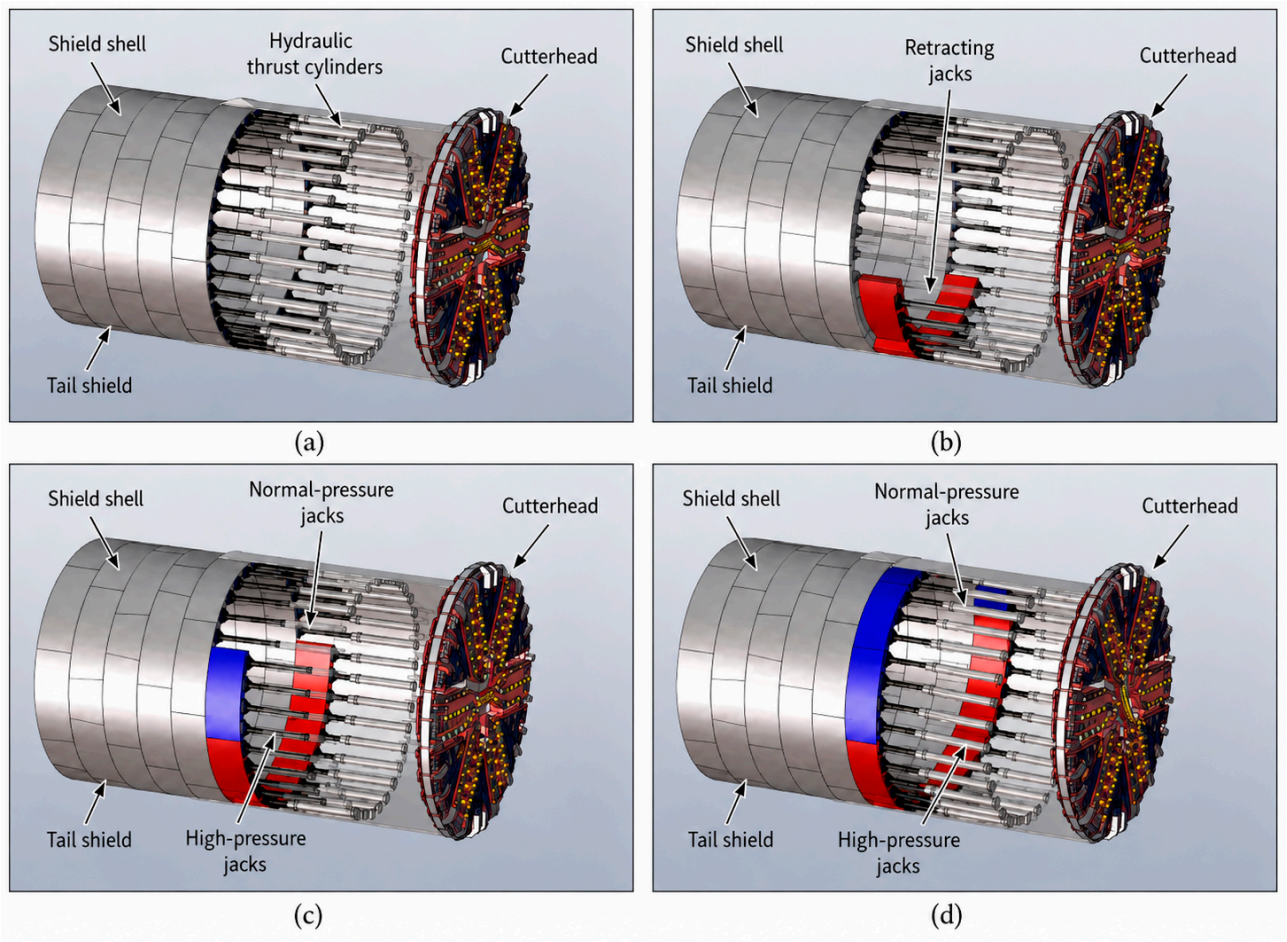


Figure 4. Schematic diagram of thrust force redistribution under STAT mode: (**a**) parameter initialization of synchronous jacking; (**b**) coordinated control of synchronous jacking; (**c**) thrust coordination control; (**d**) steady-state control of synchronous jacking.

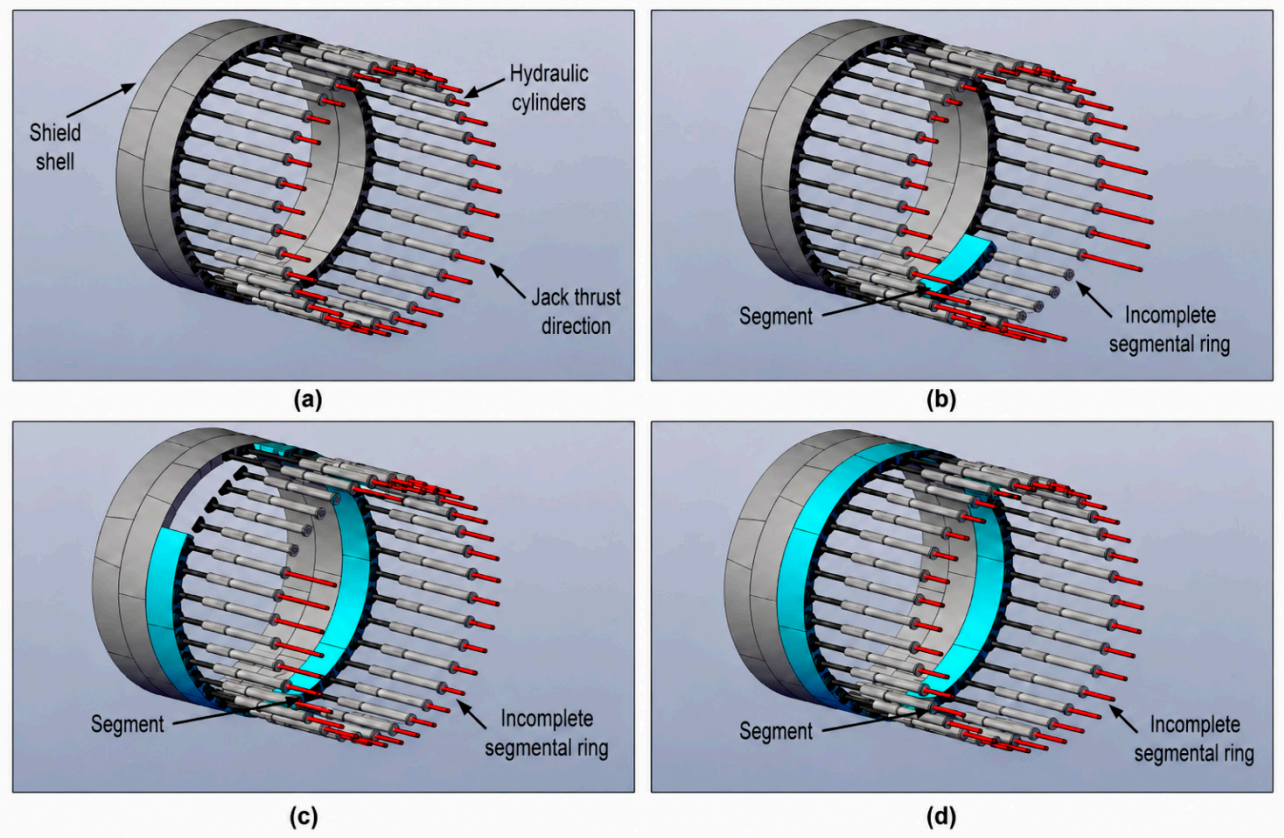


Figure 5. Pressure distribution of shield machine hydraulic cylinders under synchronous assembly–propulsion conditions: (**a**) full circumferential thrust equilibrium stage; (**b**) asymmetric thrust regulation stage; (**c**) synchronous excavation–segment erection stage; (**d**) thrust system state reset stage.

The shield machine transitions to STAT mode under verified safe operating conditions. Under ideal operational parameters, the machine advances at a rate of 30 mm/min, with individual segment assembly requiring approximately 5 min. By implementing STAT, the segment assembly time per ring is reduced by 35 min (construction efficiency increased by nearly 30%), significantly enhancing tunneling efficiency while imposing stricter requirements on the material transport system [31,32].

3. Overall Program Design

This study proposes a systematic methodological framework to establish attitude control criteria for large-diameter shield tunneling under STAT, focusing on load effects and the damage-deformation mechanisms of unclosed segment rings (including bolts) under asymmetric stress states. A finite element model was developed to calculate the critical deflection angles of unclosed segment rings subjected to high thrust forces during assembly, incorporating nonlinear contact mechanics at bolt–segment interfaces. Field load tests on bolts were conducted under STAT conditions, quantifying stress redistribution patterns and preload attenuation rates through strain gauge arrays and digital image correlation. The critical differential jack stroke was derived from the shield machine's maximum design turning radius and shield tail clearance. By integrating these parameters, comprehensive attitude control criteria were established to optimize STAT safety.

Under STAT conditions, segment rings are prone to asymmetric stress states, which concurrently affect the mechanical behavior of connecting bolts. The asymmetric stress distribution in unclosed segment rings during assembly primarily originates from two sources: positional asymmetry and external load inclination-induced asymmetry. To investigate

these effects, finite element numerical simulations of actual segment configurations were conducted to quantify stress redistribution under asymmetric loading. Complementary mechanical analyses, including numerical modeling and field tests, were performed on bolts to validate the structural safety of both segments and bolts under such asymmetric conditions. By integrating these findings with the critical differential jack strokes corresponding to the shield machine's maximum turning radius, comprehensive attitude control criteria were established (Figure 6).

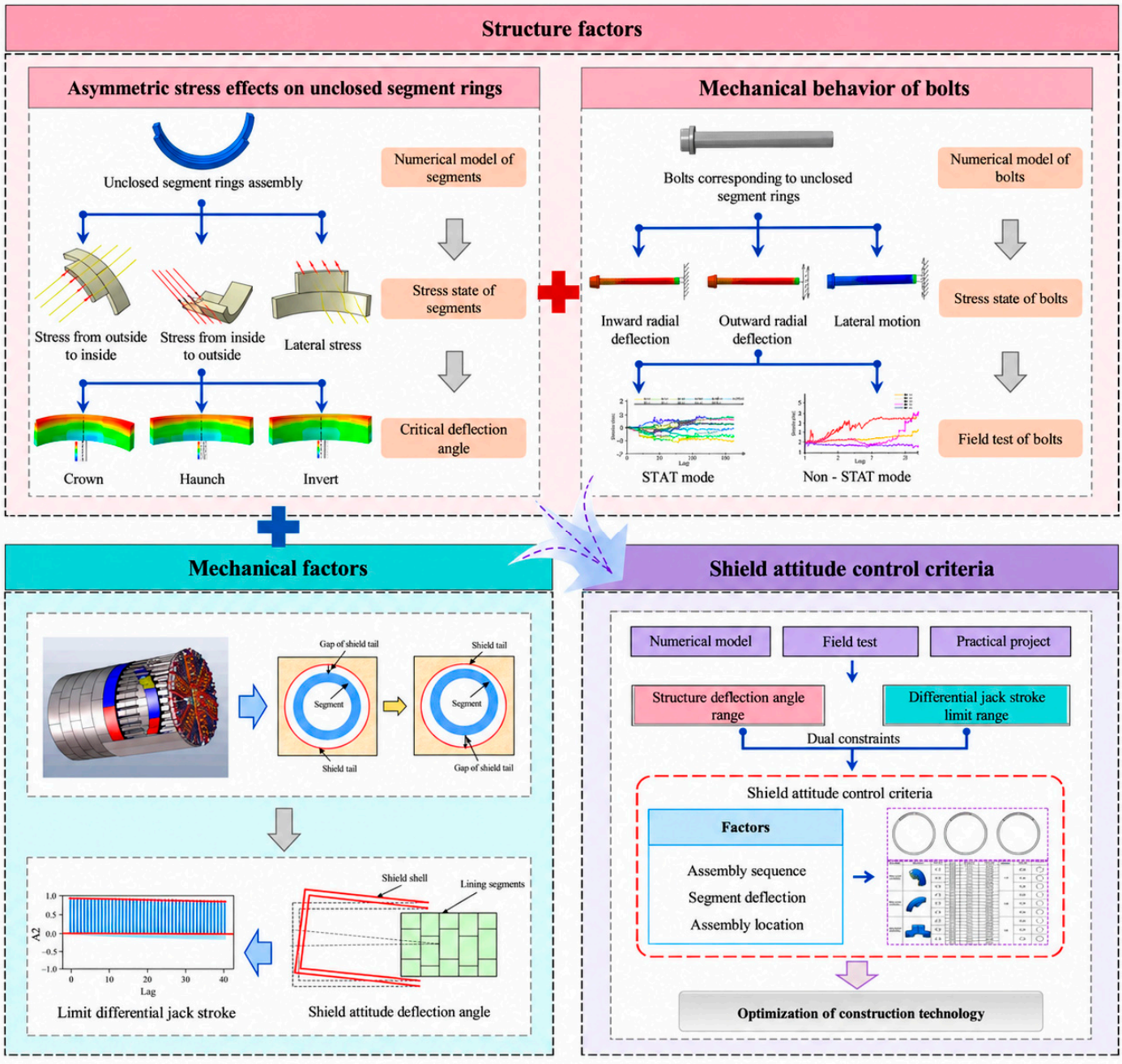


Figure 6. Overall research workflow integrating numerical simulation, field validation, and attitude control criteria.

3.1. Asymmetric Stress Effects on Unclosed Segment Rings

During STAT in large-diameter shield tunneling, unclosed segment rings are subjected to external loads comprising jack thrust and self-weight. The asymmetric stress states in segments primarily arise from angular misalignment between segments and jacks, which

is caused by suboptimal shield machine attitude during construction. Numerical simulations in this study assume the initial position of unclosed segments to be parallel and suspended relative to closed rings. Attitudinal deviations in segments are modeled by converting alignment errors into radial and tangential force components exerted by jacks. The allowable deflection range for segments is defined based on the maximum angular deviation between the shield and segments and the critical differential jack stroke derived from shield kinematic constraints. To analyze asymmetric mechanical responses, the FE model simulates actual loading scenarios while accounting for bolt-induced inter-segment constraints. This approach systematically investigates the stress redistribution patterns and damage evolution mechanisms of segments under asymmetric and locally eccentric loading conditions inherent to STAT.

1. Model establishment

A tunnel segment model was developed based on the Shanghai Rail Transit Airport Link Line (Western Section) project, employing finite element methods for refined structural modeling. Bolt holes corresponding to critical connections were selectively incorporated into the segments to analyze stress states between newly assembled rings. During the STAT process, jack thrust forces directly act on segments, which are temporarily secured in position before bolts and embedded inserts are fixed using sleeve couplers. The detailed segment configuration is illustrated in Figure 7.

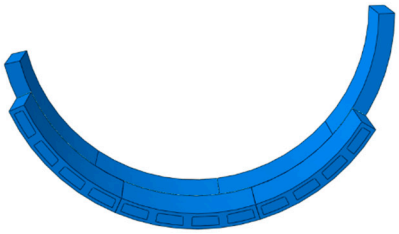


Figure 7. Schematic of model geometry.

2. Parameter selection

This study primarily utilizes FE modeling to investigate load transfer mechanisms between segments, bolts, and ancillary components. Three-dimensional models of segments, cushion layers, and waterstop rubber gaskets were developed, with concrete behavior simulated using an elastoplastic damage constitutive model. Key material and geometric parameters are provided in Tables 1 and 2. The assembly process of three interconnected segments was simulated under the most adverse conditions (maximum burial depth) to evaluate STAT-induced damage. By imposing tilt angles aligned with axial forces, damage progression was analyzed in both single- and multi-segment configurations (up to three segments, accounting for bolt-induced angular constraints). The simulation results reveal asymmetric damage patterns and localized failure mechanisms under eccentric loading inherent to STAT.

3. Numerical implementation and contact settings

To improve the reproducibility of the finite element analysis without changing the original modeling framework, additional details regarding the numerical implementation, contact settings, and convergence control were added in the revised manuscript. The concrete segments, cushion layers, and waterstop rubber gaskets were discretized using three-dimensional solid elements, while local mesh refinement was applied around bolt holes, segment joints, contact interfaces, and regions subjected to jack thrust, where stress concentration and damage initiation were expected. The mesh density adopted in the

simulations was selected to ensure stable stress transfer and contact behavior in the key local regions of the segment–bolt system.

Table 1. Geometric parameters of model inputs.

Input Parameters	Value
Diameter of tunnel (m)	13.6
Standard thickness of segments (mm)	550
Standard length of segments (m)	2.03
Standard angle of segments (°)	42.35
Number of rubber strips per segment (pcs.)	1
Number of nitrile cork liners per segment (pcs.)	1
Thickness and width of waterstop rubber strips (mm)	20 and 70
Nitrile cork liner thickness and width (mm)	5 and 300
Standard number of segment ring bolts (pcs)	4
Standard number of segment longitudinal bolts (pcs)	3

Table 2. Material parameters of model.

Input Parameters	Value
Density of concrete (kg/m^3)	2450
Young's modulus of concrete (GPa)	36
Poisson's ratio of concrete (-)	0.2
Stiffness of bolt system (kN/mm)	9.18
Density of bolt (kg/m^3)	7850
Young's modulus of bolts (GPa)	200
Poisson's ratio of bolts (-)	0.3

Contact interactions were defined between adjacent segment surfaces, segment–cushion interfaces, and segment–waterstop rubber gasket interfaces. A surface-to-surface contact formulation was adopted to describe the interaction between these components. Normal contact behavior was defined using hard contact to prevent mutual penetration under compression, while tangential behavior was described using a penalty friction formulation to allow for limited relative sliding along the interfaces. The bolt–embedded insert connection was represented using mechanical coupling constraints so that the load transfer between bolts and segments could be captured while maintaining numerical stability.

The nonlinear finite element analysis was performed using an implicit solver. Geometric nonlinearity was considered because segment deflection, interface separation, and contact state changes occurred during the assembly process. The jack thrust was applied incrementally to improve convergence stability. During the simulations, convergence was controlled by the residual force and displacement criteria of the nonlinear solution procedure. No severe element distortion, abnormal contact penetration, or non-convergent response was observed in the adopted models, indicating that the numerical results were stable for the modeling strategy used in this study.

It should be noted that a complete mesh independence study with coarse, medium, and fine meshes was not included in the present revision because it would require additional full-scale nonlinear contact simulations for all assembly positions and loading scenarios.

Considering the high computational cost and the engineering focus of this study, the current revision instead supplements the numerical implementation details and explicitly acknowledges this limitation. Future work will further conduct systematic mesh sensitivity analysis and parametric numerical stability evaluation to quantify the influence of mesh density and contact parameters on the predicted segment damage thresholds and bolt stress responses.

4. Boundary condition

During segment assembly, the initial positioning of the first segment undergoes periodic rotation due to its tapered geometry, which is the primary cause of positional asymmetry. Jack thrust forces exhibit gradient escalation with increasing tunnel depth in STAT, resulting in non-uniform load distribution across individual segments. Additionally, distinct boundary conditions and constraints are applied to segments at different assembly positions.

Under STAT conditions, segments are subjected to external loads comprising jack thrust and self-weight. The asymmetric stress distribution manifests as angular misalignment between segments and jacks, primarily caused by suboptimal shield attitude during construction (Figure 8). The allowable deflection range is governed by two critical parameters: the maximum angular deviation between shield and segments and the critical differential jack stroke derived from shield kinematic limits. The assembly process involves complex segment–cushion–segment interactions. Compared to unclosed segment rings, closed rings exhibit reduced relative displacements due to hoop effects generated by annular structural interactions, effectively constraining deformation.

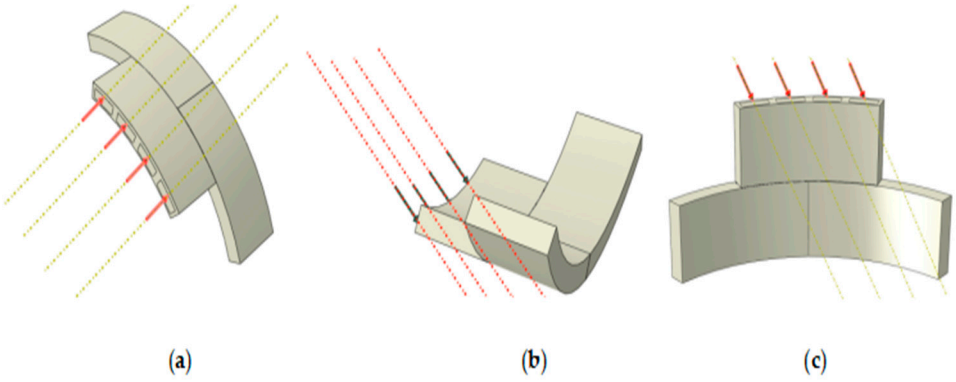


Figure 8. The relationship between the stress direction of the segment and the jack: (**a**) The force of the jack from the outside in. (**b**) The force of the jack works from the inside out. (**c**) Lateral force.

3.2. Mechanical Behavior of Bolts Corresponding to Unclosed Segment Rings

3.2.1. Numerical Simulation of Bolts

After segment assembly, the progressive advancement of jacks induces dynamic changes in bolt stress states. Given the critical role of bolt integrity in overall tunnel safety, numerical simulations of bolt mechanical behavior are imperative. The simulation setup is detailed in Figure 8a.

The numerical modeling of bolts under STAT conditions was conducted to quantify stress evolution. By incorporating failure angles at distinct segment locations and assembly sequences, this study analyzes radial and lateral stress redistribution in bolts during deflection events. This approach enables a systematic evaluation of bolt safety thresholds during segment failure initiation.

A deflection angle of 2° was prescribed as a comparative numerical loading case to examine bolt stress responses under inward radial, outward radial, and lateral deflection

modes. This prescribed angle was selected for consistent comparison among the three loading modes and should not be interpreted as a critical segment failure angle or an allowable construction limit.

3.2.2. Field Test of Bolts

1. Content and purpose of test

In tunnel construction, lining structures are categorized into circumferential bolts and longitudinal bolts based on their spatial orientation. This experimental study comprises two components. (a) Single-segment testing: In order to determine the normal bolt axial force and bending moment transfer distribution, according to the different positions of the bolt, a circumferential bolt test and longitudinal bolt test can be used. (b) STAT ring testing: In order to determine the distribution of bolt axial force and bending moment transfer under the synchronous thrust and assembly mode, a circumferential bolt test and longitudinal bolt test can be used according to the different positions of the bolts. By varying tilt angles and loading conditions, damage progression was investigated in both single-segment and multi-segment configurations (clusters of up to three segments, incorporating angular constraints imposed by inter-segment bolts).

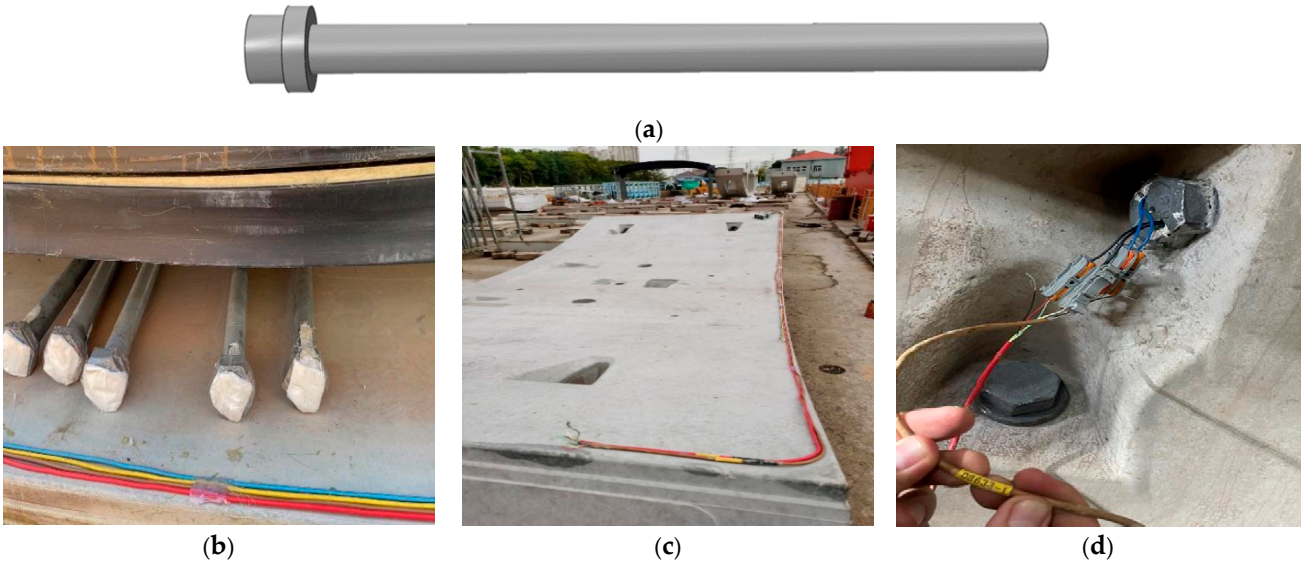
Bolts represent critical weak points in shield tunnel lining rings, with their mechanical performance significantly influencing the overall structural behavior of the lining system [33–36]. Unlike conventional shield tunneling, this metropolitan railway tunnel project employs large-diameter shield tunneling combined with the innovative STAT method. To ensure the safety and rationality of lining design, it is imperative to clarify bolt mechanical behavior under STAT conditions. This investigation aims to validate parameter selection in structural calculations and construction design while proposing quality control requirements and optimization strategies to achieve optimal technical and economic benefits. Bolt stress was measured using strain gauges. Specialized bolt instrumentation was implemented (symmetrical grooves were machined at the bolt tail ends, with strain gauges precisely mounted within the grooves).

2. Test specimen and equipment

The bolts employed in this project are Grade 8.8 high-strength bolts with a yield strength of 640 MPa. In the bolt–segment model, bolts were fixed to corresponding embedded bolt hole inserts using tie constraints to simulate realistic mechanical interactions. The data acquisition system utilized the DH3823 distributed signal testing and analysis system, comprising three core components: an Ethernet switch, power controller, and data acquisition units. The testing system was configured by connecting computers to DH3823 distributed data loggers through power or communication cables, signal input cables, Ethernet cables, and a POE switch, forming an integrated measurement network.

3. Test procedure

The test segments were pre-positioned by the experimental team, with sensor wires pre-stripped and secured along segment edges. Temporary protective covers were applied to prevent wire damage during hoisting and transportation (Figure 9a). Instrumented bolts, pre-fitted with strain gauges, were radially aligned and lowered with segments (Figure 9b). Data acquisition cables were circumferentially arranged, as illustrated in Figure 9c. Due to on-site constraints and construction schedule limitations, rapid test setup was conducted during intermittent pauses in segment installation and shield thrust. The data acquisition software used was initialized and tested in advance to ensure system integrity. Post-assembly, junction boxes pre-connected to measurement channels were mounted on segments using custom brackets, with all cable connectors systematically engaged.



(**a**)

(**b**) (**c**) (**d**)

Figure 9. Test configuration diagram: (**a**) Bolt model. (**b**) Bolt wrapping. (**c**) Arrangement of data acquisition lines. (**d**) Bolt strain gauge wiring.

To optimize time efficiency during bolt installation, the rapid wiring of strain gauges was prioritized. Each bolt head was equipped with four terminals, grouped into pairs corresponding to individual data acquisition (DAQ) channels. DAQ cables were securely fastened using quick-connect clamps (Figure 9d), with this standardized procedure applied uniformly across all bolts. Each DAQ cable was systematically labeled to match its assigned bolt identifier. Upon the completion of all connections, the computer-based DAQ system initiated continuous data recording, ensuring the comprehensive archival of stress–time histories. Following data acquisition, all instrumentation was sequentially disassembled.

Due to the uninterrupted STAT construction process, limited installation time, and restricted access to several bolt locations, only Ring 1488 was instrumented. Therefore, the field measurements were used as case-based engineering evidence rather than as a statistically representative dataset.

3.3. Acquisition of Differential Jack Strokes Corresponding to Shield Machine Deflection Angles

In STAT mode, the asymmetric stress effects on unclosed segment rings were analyzed through numerical simulations. Critical failure angles were determined based on these simulations. Furthermore, a finite element model of connecting bolts was developed to investigate their mechanical behavior under STAT conditions, with validation via field tests confirming bolt integrity under non-destructive states. Interactions between adjacent segments were analyzed under varying deflection angles, converting these angles into corresponding differential jack strokes. These values were then compared with the shield machine's kinematic limits to verify the feasibility of critical failure angles. The analysis confirmed that segment damage initiates when deflection angles exceed tolerance thresholds derived from jack stroke differentials.

During STAT operations, deviations in shield machine attitude critically influence segment loading. Misalignment between jacks and segments induces compounded geometric discrepancies between the shield and lining. As illustrated in Figure 10, the angular deviation between the shield axis and segment axis can be calculated from differential jack strokes using established geometric relationships:

$$\delta = D \sin \alpha = \frac{D_w + D_n}{2} \sin \alpha \quad (1)$$

where δ is the differential stroke between the upper and lower jack groups or between the left and right jack groups; α is the angular deviation between the shield axis and the segment axis; D is the effective jack-zone diameter; and D_w and D_n are the outer and inner diameters of the segmental lining, respectively.

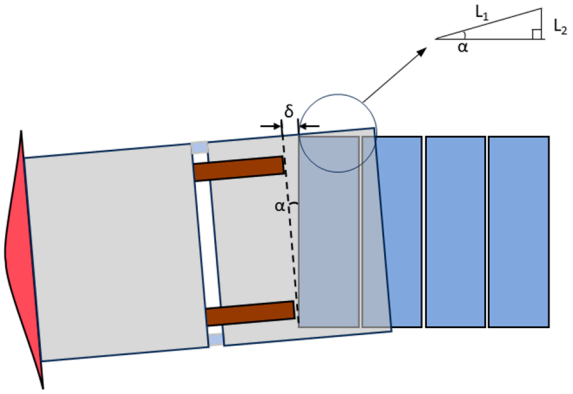


Figure 10. Differential jack stroke and shield turning angle: α, shield–segment angular deviation; δ, differential jack stroke; L_1, effective longitudinal distance to the shield tail; L_2, shield-tail clearance. The dashed line marks the shield end plane; the circle and arrow indicate the enlarged region; the square denotes a right angle. Gray: shield; brown: jacks; blue: lining; red: cutterhead.

Equation (1) represents a simplified planar kinematic relationship. It assumes rigid-body rotation and coplanar shield and segment axes and uses the mean segment diameter as the effective distance between opposite jack zones. The elastic deformation of the shield, jack clearance, shield–soil interaction, and operational disturbances are not included. Therefore, the calculated differential jack stroke represents a deterministic geometric estimate rather than the actual stroke variation under all field conditions.

During shield tunneling construction, the dynamic attitude deviation in the shield machine significantly influences the stress state of segment structures. Under STAT conditions, such deviations may induce severe engineering hazards. When the jack thrust forces exhibit uneven distribution (non-axisymmetric with angular bias) or the differential jack strokes exceed design tolerances, the relative positional relationship between the shield machine and segments undergoes substantial tilting. This not only induces stress concentration at segment joints and amplifies joint misalignment but may also trigger localized concrete cracking or even structural instability. Therefore, the real-time monitoring and adjustment of shield attitude deviations (including axial deviation angles and differential jack strokes) are critical for ensuring STAT construction quality. By constraining the shield machine's actual turning angles, construction risks can be effectively mitigated, thereby enhancing the safety and durability of tunnel structures.

3.4. Construction of Shield Attitude Control Criteria Under STAT Mode

The formulation of shield attitude control criteria is based on a dual-constraint analysis involving segment deflection angles and critical differential jack strokes. Specifically, quantitative control metrics can be established through two complementary mechanical mapping relationships. Segment deflection angles (including joint bolt stress states) are monitored to inversely derive jack stroke differentials, which are then compared with design tolerance thresholds. Jack stroke differentials are computationally extrapolated to predict segment deflection angles, which are evaluated against critical deflection thresholds.

Both methods provide foundational criteria for engineering controls, with core metrics encompassing segment deflection angles and jack stroke differentials. Regardless of the primary metric, the process constitutes an optimized constraint analysis, ensuring segments

remain within elastic stress states during assembly. This prevents structural damage induced by localized stress concentrations or joint misalignments. By establishing coupled mechanical mapping relationships between these dual metrics, the framework enables comprehensive and precise dynamic adjustments of shield attitude. This approach significantly enhances segment assembly quality and structural safety in tunnel engineering.

Critical failure angles vary across different segment locations during assembly simulations. The results indicate that segments initiate failure the earliest during outward radial deflection. To ensure construction safety, segment integrity must be preserved at every assembly stage. Figure 11 illustrates the mechanical responses and geometric parameters during simulated deflection. The following can be obtained based on geometric relationships:

Radial deflection:

$$\delta = L_3 \sin\beta \tag{2}$$

Lateral deflection:

$$\delta = L_4 \sin\beta \tag{3}$$

where L_3 denotes the vertical distance between the segment base and arc crown, and L_4 represents the segment chord length (Figure 12). The segment deflection angle can be converted into a controlled differential jack stroke value. Additionally, collision risks between deflecting segments and the shield shell must be evaluated via Figure 11b. This allows for the translation of shield angular deviation into permissible jack stroke differential limits, which are subsequently adopted as attitude control criteria for large-diameter shield tunneling under STAT conditions.

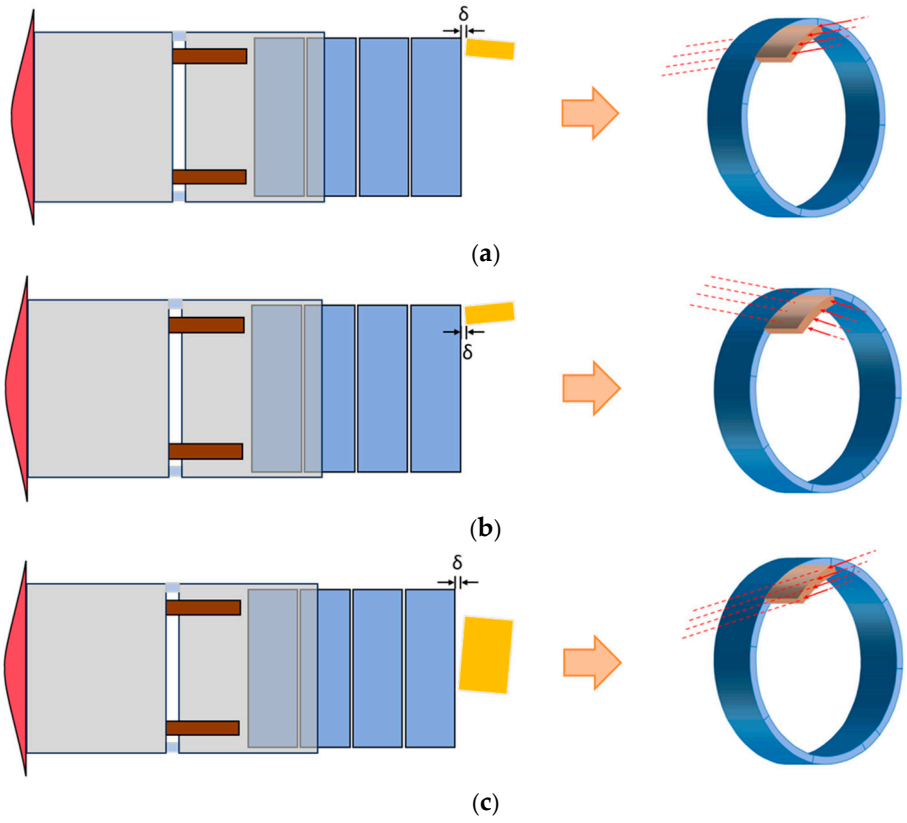


Figure 11. Deflection and stress analysis during the assembly of segments: (**a**) Radial inward deflection. (**b**) Radial outward deflection. (**c**) Deflection along the side of the tunnel.

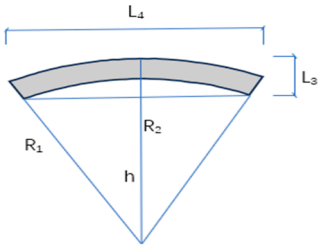


Figure 12. The geometric parameters of the segment: R_1, inner radius; R_2, outer radius; h, perpendicular distance from the ring center to the segment-base chord; L_3, vertical distance between the segment base and arc crown; and L_4, segment chord length.

The differential jack strokes of 0.7 cm and 11.7 cm were obtained by substituting the minimum radial and lateral damage initiation angles into Equations (2) and (3), respectively. These values represent conservative structural control limits among the investigated assembly conditions. In contrast, 21.9 cm represents the kinematic upper limit derived from the shield geometry and design turning condition, rather than the structural safety limit.

4. Research Results

The mechanical behavior of unclosed segment rings under asymmetric stress conditions remains inadequately characterized during STAT. A comprehensive understanding of load effects during asymmetric assembly is therefore critical. Numerical simulations were developed to analyze stress responses and damage mechanisms under actual engineering constraints. Beyond jack thrust forces, gravitational effects on segments vary depending on their spatial orientation, inducing distinct rotational tendencies. Consequently, the coupled interactions between gravity and jack thrust must be rigorously evaluated in STAT processes. To address this, a three-segment assembly sequence was modeled using finite element analysis. The 3D FE model explicitly simulates segments, cushion layers, and sealing gaskets, enabling the direct observation of mechanical behavior and damage evolution during assembly.

During segment assembly, segments undergo deflection under jack thrust forces, resulting in angular misalignment between newly installed segments and previously assembled rings. Beyond thrust forces, inter-segment contact quality directly governs final segment alignment. Curved segments exhibit distinct rotational tendencies under gravitational effects depending on their spatial orientation, which further induces bending deformations. This study focuses on the coupled mechanical interactions during STAT assembly, where segments are subjected solely to gravity and jack thrust forces.

4.1. Calculation and Analysis of Segments

4.1.1. Radial Interaction

Under jack thrust forces, segments undergo deflection during assembly, creating angular misalignment with adjacent rings. The gravitational-induced deflection varies significantly depending on segment positioning. The finite element model adopts a consistent N–mm–MPa unit system; therefore, all displacement values shown in Figures 13–15 are expressed in millimeters and are not normalized:

1. Crown position assembly: Segments exhibit inward rotation due to the asymmetric compression of waterstop rubber gaskets and cushion layers. STAT-induced thrust forces drive the segment toward closed rings, resulting in the greater internal deformation of gaskets compared to external regions (Figure 13).

2. Haunch position assembly: Segments similarly deflect inward but with asymmetric load distribution disrupting structural symmetry. This asymmetry arises from differential ground reaction forces on the segment's curved geometry (Figure 14).
3. Invert position assembly: When the initial assembled segment is at the bottom compared to the first segment assembled at the top and side, the tendency of the push-on end of the segment toward inward deflection is the lowest (Figure 15).

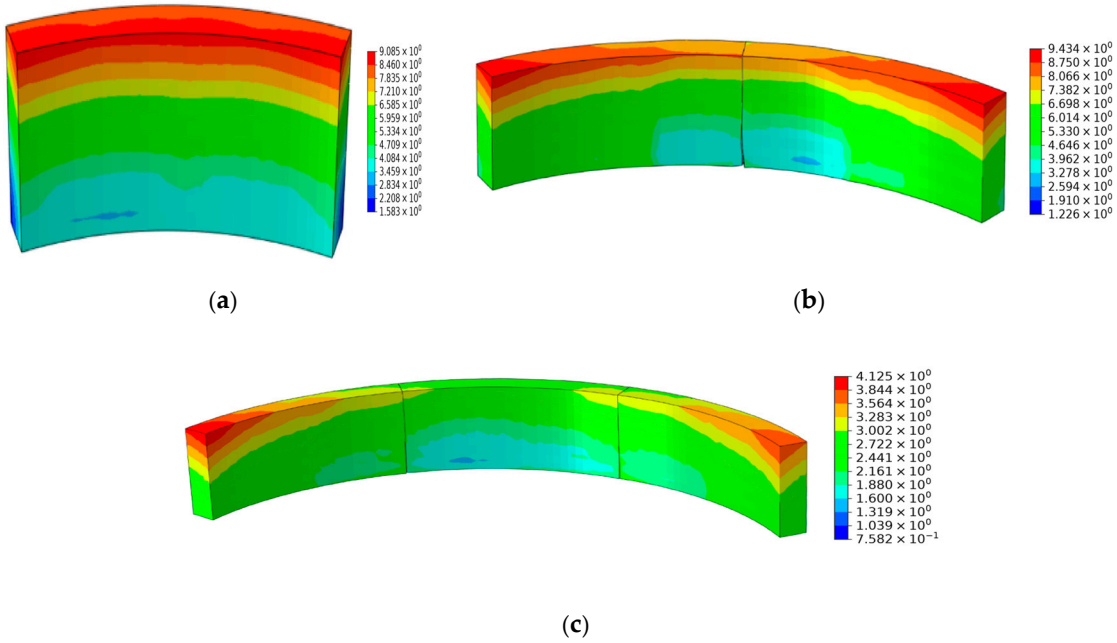


Figure 13. Interaction and displacement of crown position assembly: (**a**) First segment assembly. (**b**) Second segment assembly. (**c**) Third segment assembly. Displacement unit: mm.

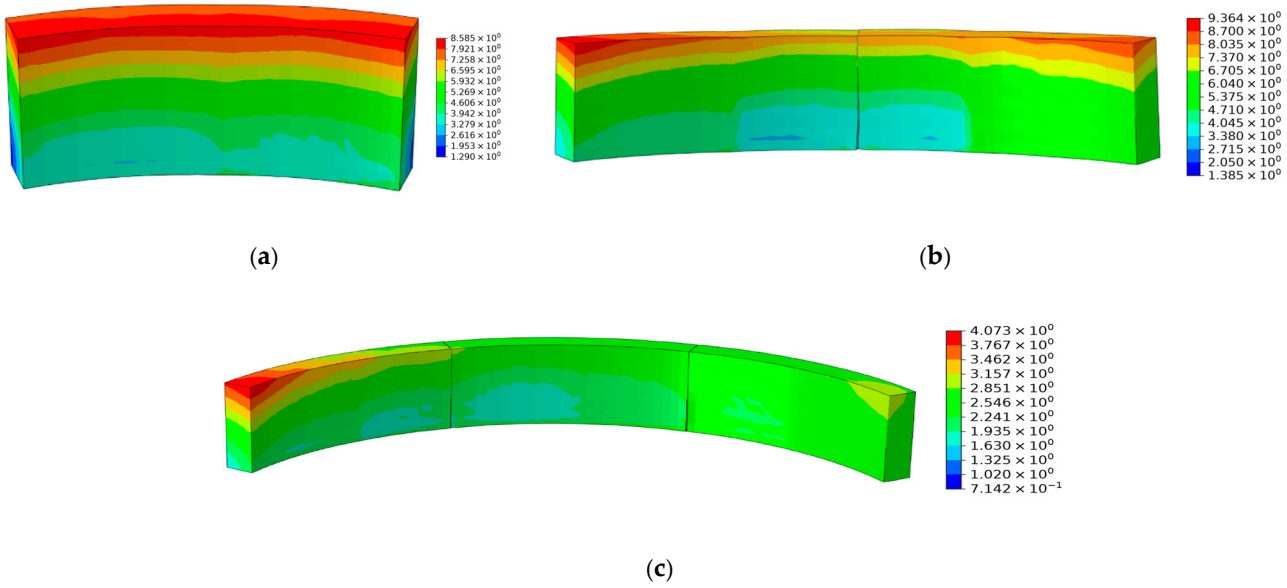


Figure 14. Interaction and displacement of haunch position assembly: (**a**) First segment assembly. (**b**) Second segment assembly. (**c**) Third segment assembly. Displacement unit: mm.

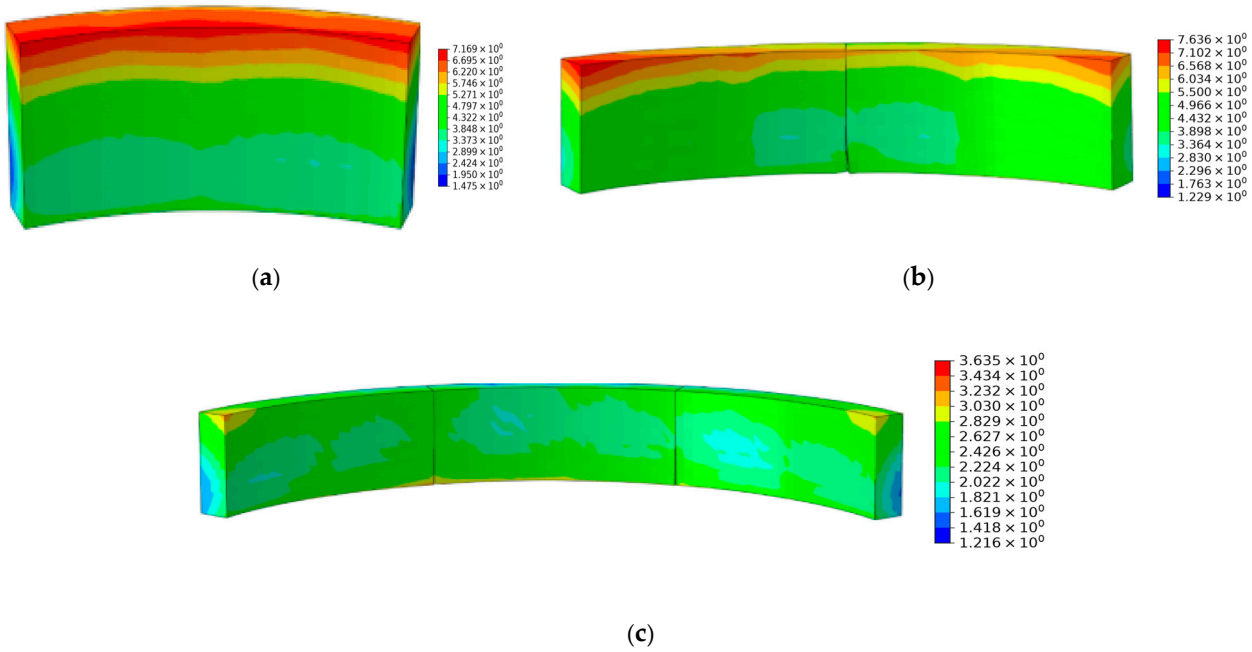


Figure 15. Interaction and displacement of invert position assembly: (**a**) First segment assembly. (**b**) Second segment assembly. (**c**) Third segment assembly. Displacement unit: mm.

4.1.2. Axial Interaction

Throughout this study, no direct contact between segments was observed, aligning with actual assembly conditions where gaps are maintained by cushion layers and waterstop rubber gaskets. Asymmetric stress states induced by shield attitude deviations manifest as two distinct modes: radial deflection and lateral deflection. Segments exhibit radial inward deflection or radial outward deflection, primarily influenced by initial positional errors (assembly misalignment) between the shield and segments. Segments undergo lateral tilting, directly attributed to differential jack strokes exceeding geometric tolerance thresholds.

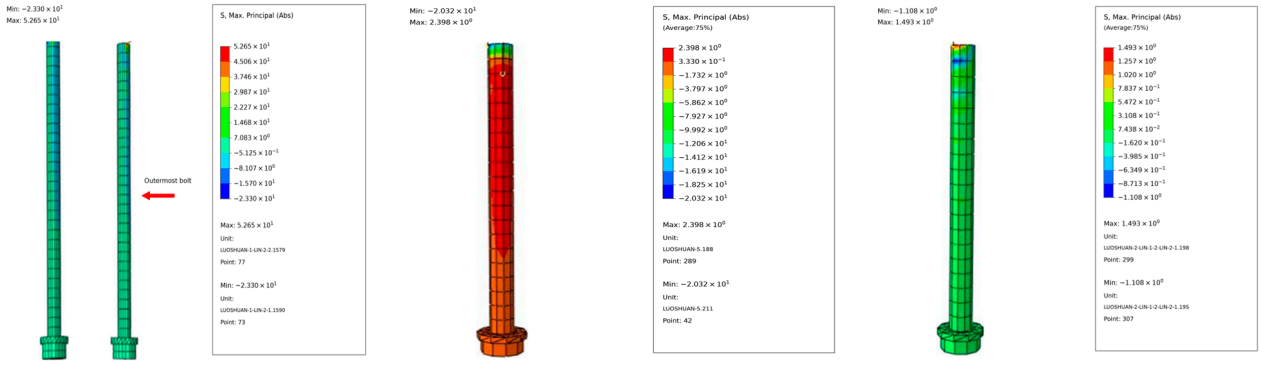
4.2. Calculation and Analysis of Bolts Based on Segment Deflection

4.2.1. Inward Radial Deflection

During single-segment assembly, only four longitudinal bolts are engaged. The maximum bolt stress occurs at the bolt–segment contact zones, where localized stress concentrations are observed. The detailed thread geometry was not explicitly modeled, and the bolt–insert connection was idealized using a coupling constraint. Therefore, the analysis focuses on the global stress response of the bolt shank rather than local thread-root stresses or interface slip. The calculated peak stresses may consequently be underestimated and should not be interpreted as direct predictions of thread failure. As shown in Figure 16a, when the initial segment is positioned at the haunch, the two right-side bolts exhibit the highest shank stresses. Specific regions of the bolts experience compression aligned with segmental squeezing under gravitational effects, while tension occurs near bolt–segment interfaces, likely due to localized stress concentrations.

During the assembly of two adjacent segments, circumferential bolts are engaged. The maximum compressive or tensile stresses in bolts occur when the first segment is positioned at the invert. Under inward deflection, circumferential bolt shanks predominantly exhibit minor tensile stresses. Localized compression is observed near the threaded regions (Figure 16b shows the lowermost circumferential bolt), likely due to contact forces with concrete. The clamping effect from dual-segment assembly alleviates compressive stresses in longitudinal bolts. The positioning of segments has negligible influence on bolt stresses

during two-segment assembly. The highest stresses in longitudinal bolts manifest in the four outermost bolts between the two segments, where compressive forces dominate—consistent with the segment displacement patterns described in prior sections. During third segment assembly (Figure 16c), reduced segment mobility due to geometric constraints results in more uniform stress distribution, with mitigated compression/tension extremes. Minor stress concentrations persist at shank–thread transition zones.

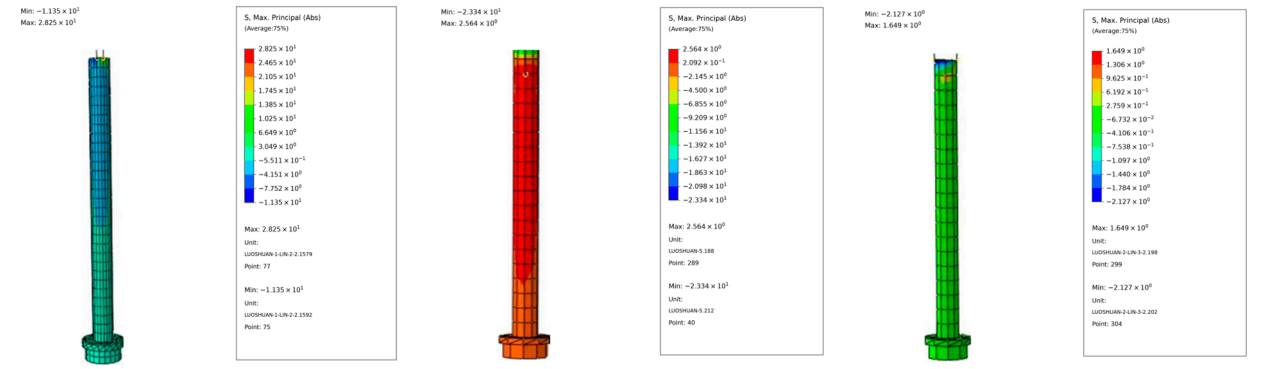


(**a**) (**b**) (**c**)

Figure 16. Stress on the bolt when the initial segment is in the upper part deflected inwards by 2°: (**a**) First segment assembly. (**b**) Second segment assembly. (**c**) Third segment assembly.

4.2.2. Outward Radial Deflection

When the first segment is assembled at the invert and subjected to outward radial deflection, compressive stresses dominate in the bolt shanks, with the outermost bolts experiencing the highest compression (Figure 16a). At the invert, segments exhibit the most severe outward deformation, resulting in the maximum bolt stresses under outward radial deflection. Figure 17b,c demonstrate that the lowermost circumferential bolts in two- and three-segment assemblies exhibit peak stress concentrations. During two-segment assembly, stress distribution remains relatively uniform, with localized compression observed only on the threaded sides of bolts. The engagement of circumferential bolts mitigates outward deflection, thereby reducing stress severity in longitudinal bolts. Under outward radial deflection, the calculated global bolt-shank stresses remained below the yield strength; however, local thread-root stresses were not evaluated.

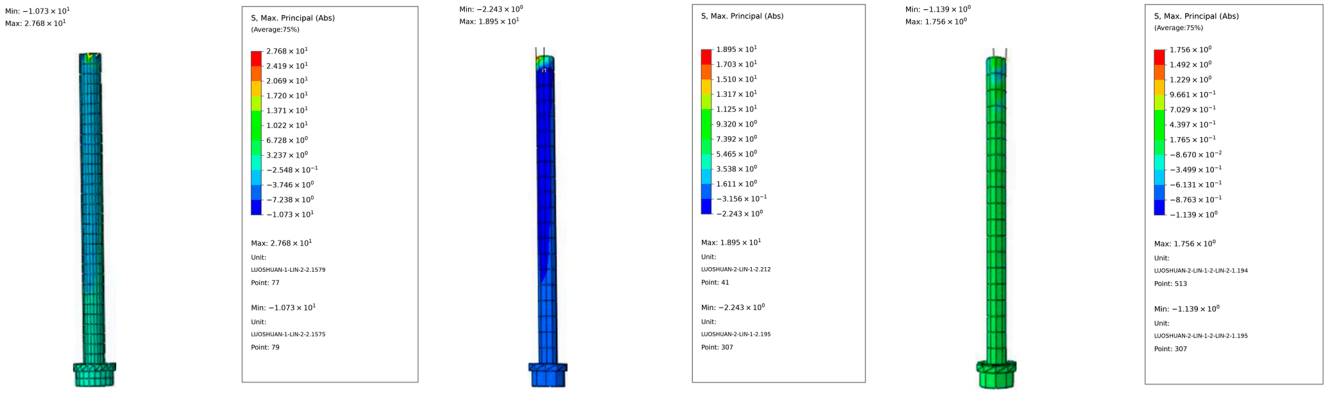


(**a**) (**b**) (**c**)

Figure 17. Stress on the bolt when the segment is deflected outwards by 2°: (**a**) First segment assembly. (**b**) Second segment assembly. (**c**) Third segment assembly.

4.2.3. Lateral Deflection

After the first segment is assembled, bolts primarily experience compressive stresses under lateral deflection, with the maximum stress concentrations localized on the compression side of the segment (as shown in Figure 17a). Following the assembly of the second segment, compressive stresses in bolts are mitigated, resulting in more uniform stress distribution across bolt shanks. However, the maximum stress positions remain consistent with those observed during single-segment assembly, occurring in longitudinal bolts (Figure 18b,c).



(**a**) (**b**) (**c**)

Figure 18. Stress on the bolt when the segment is on the waist side at a deflection of 2°: (**a**) First segment assembly. (**b**) Second segment assembly. (**c**) Third segment assembly.

4.3. Analysis of Bolt Test

To validate the reliability of the simulation results, in situ engineering tests were conducted to verify the accuracy of theoretical and numerical models. The experimental protocol prioritized monitoring the mechanical responses of segments and bolts, including: bolt stress–strain behavior using embedded strain gauges, inter-segment gap variations measured via laser displacement sensors and load-bearing capacity thresholds under maximum and operational pressures. These metrics ensured structural stability during assembly (experimental setup detailed in Figure 19).

The tests were implemented within the Shanghai Regional High-Speed Rail Link project, focusing on bolt mechanics under STAT. Bolts were instrumented with symmetrical machined grooves and planar surfaces (Figure 19e). Strain gauges were bonded to bolt shanks using epoxy adhesive, followed by silicone encapsulation for environmental protection. Segment No. 1488 was selected for instrumentation, with DAQ systems and cabling pre-installed at the invert to capture real-time stress data.

Given the time-saving nature of STAT operations, which enable continuous segment assembly without pauses, and considering the large tunnel diameter of 14 m that rendered some bolt locations inaccessible, this experiment focused solely on post-assembly bolt stress measurements after two-segment synchronization. The tested segment was positioned at the invert (Ring 1488), with shield attitude deviations recorded as follows during thrust. Horizontal deviations are 5 mm of shield head and 20 mm of shield tail. Vertical deviations are 34 mm of head and 29 mm of tail, inducing predominant inward radial misalignment. Therefore, the field test does not provide direct evidence of bolt integrity during the extreme single-segment loading stage, which was evaluated only through finite element analysis. Strain gauges were interfaced with data acquisition systems via quick-connect modules, ensuring rapid and reliable signal transmission despite spatial constraints.

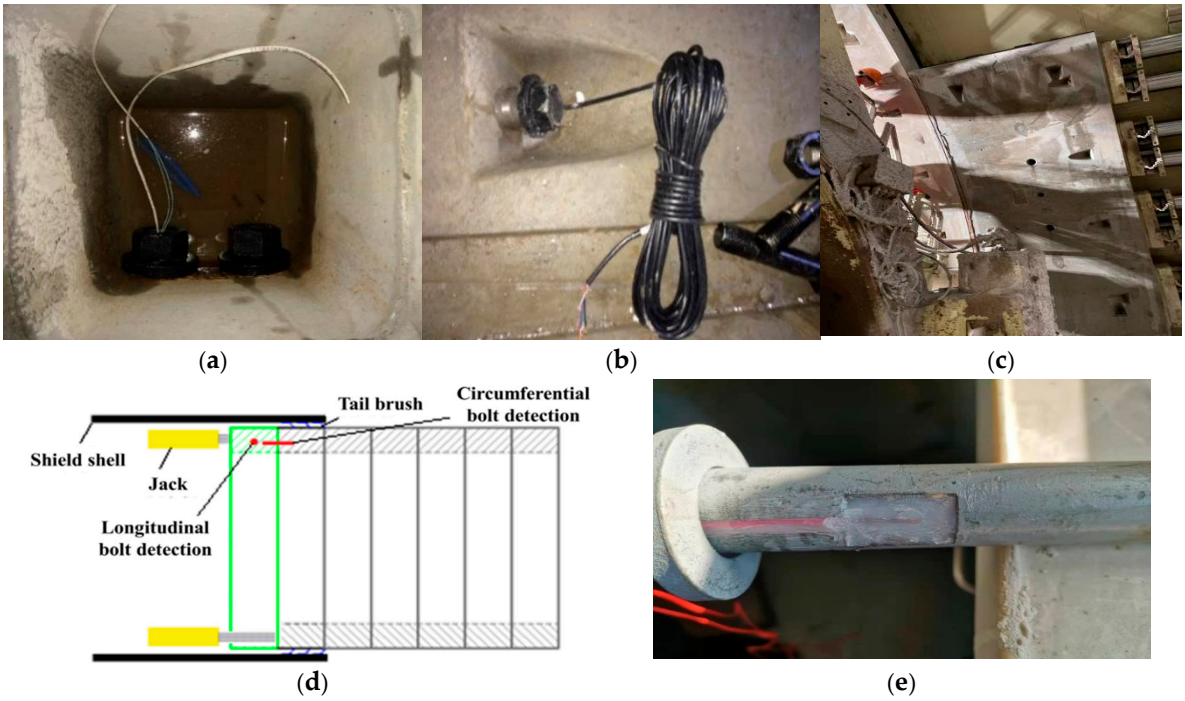


Figure 19. Facilities and arrangement of bolt test: (**a**) Circumferential bolt strain measurement points. (**b**) Longitudinal bolt axial gauge. (**c**) Test segment assembly. (**d**) Schematic diagram of bolt detection position. (**e**) Posting of strain gauges on bolts.

4.3.1. Bolt Forces in STAT Mode

Following segment installation, bolts are tensioned to generate initial preloads caused by frictional interactions between bolts and embedded inserts during impact drilling. Under STAT conditions, data acquisition commenced with the installation of segment B3 (first in sequence). Subsequent assembly phases were timed as follows: B4 (second segment) installed at 63 s, B1 (third segment) installed at 181 s, and B2 (fourth segment) installed at 391 s. This staggered assembly sequence ensured the systematic monitoring of bolt preload evolution during STAT operations.

In Figure 20, B3 and B4 denote the monitored segment identifiers. Labels B3–1 to B3–4 and B4–1 to B4–4 denote individual circumferential bolts, whereas the suffix "S" denotes longitudinal bolts; B3 S–1, B3 S–2, and B4 S–1 identify the corresponding monitored longitudinal bolts. These labels represent different instrumented bolts rather than different gauge locations on the same bolt. All strain gauges used for the plotted curves were mounted on the bolt shanks. The measured stress distribution is illustrated in Figure 20. Observations reveal that first segment bolts exhibit minor stress reduction during second segment thrust, likely due to load redistribution. Second segment bolts maintain stable stress profiles, indicating equilibrium under progressive thrust. Third segment assembly induces significant stress fluctuations caused by abrupt thrust redistribution and shield machine vibrations. However, overall stress mitigation occurs as three segments form a clamping effect, reducing bolt loads compared to dual-segment configurations. Notably, circumferential bolts in STAT exhibit minimal stress variation, confirming their structural safety under operational loads. For the monitored Ring 1488, the recorded stress variations did not exhibit abrupt escalation or bolt failure during the monitored period. However, the installation preload was not independently measured, and corresponding tightening-torque records were unavailable. Therefore, the absolute total bolt stress and the quantitative safety margin relative to the 640 MPa yield strength cannot be determined from the present

data. The field results are used only as case-based evidence of bolt stress evolution for one monitored ring.

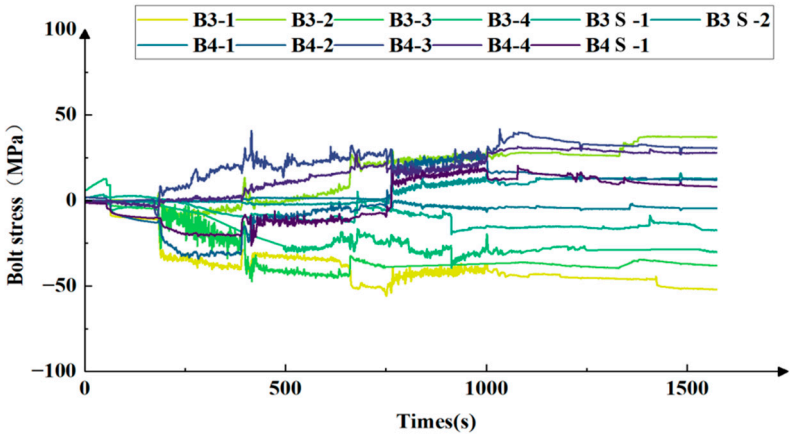


Figure 20. Bolt stress during STAT mode. B3 and B4 denote segment identifiers; numbered labels represent circumferential bolts; and "S" labels represent longitudinal bolts. All strain gauges were mounted on the bolt shanks.

4.3.2. Bolt Forces in Non-STAT Mode

This experiment conducted bolt stress testing on segments B3 and B4 under non-synchronous assembly conditions, with stress evolution profiles derived from field data (Figure 21). Bolt B3–2 exhibited minimal stress with stable behavior throughout assembly. Bolt B3–1 maintained initial stability before rising to a steady-state stress of 20 MPa. Despite both sensors monitoring the same bolt, B3–1 recorded lower magnitudes due to asymmetric load paths post-assembly. B4 bolts demonstrated initial stability followed by progressive stress escalation (peak: 15 MPa) during shield advancement, stabilizing with minor oscillations. This confirms stress equilibration under sustained thrust loads.

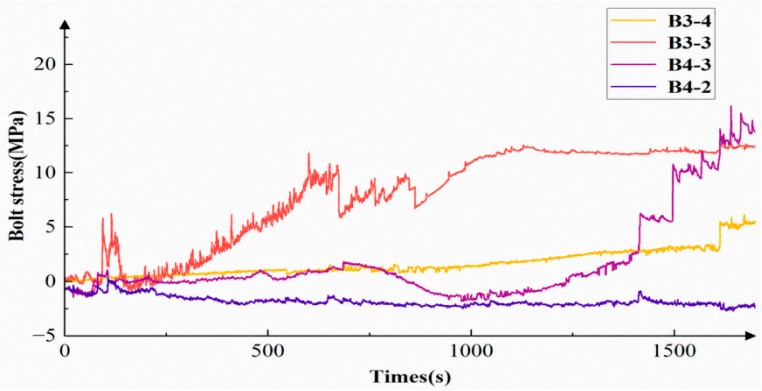


Figure 21. Bolt stress during non-STAT mode.

The overall consistency between the measured and simulated stress trends provides case-based support for the finite element model. However, the single-ring measurement does not constitute statistical validation.

4.4. Shield Attitude Deflection Angle

During shield tunneling, the deflection of the shield machine creates an angular deviation (deflection angle) between its axis and the designed tunnel alignment. This angular deviation alters the relative distances between individual jacks and the tunnel axis, generating differential jack strokes. Larger deflection angles result in more pronounced stroke

differentials. Under STAT conditions, deflection angle variations directly impact segment assembly accuracy and stress distribution, as segments are installed concurrently with shield thrust. Controlling jack stroke differentials within permissible thresholds is critical to ensuring segment assembly quality. Excessive differentials may induce segment misalignment or uneven bolt loading, compromising tunnel structural stability. In practice, the critical differential jack stroke corresponding to a given deflection angle can be calculated by integrating the shield machine's maximum design turning radius and shield tail clearance. This provides a scientific basis for real-time shield attitude control and risk mitigation.

As shown in Figure 10, L_1 is the effective longitudinal distance from the shield rotation reference point to the shield tail, and L_2 is the available transverse clearance between the shield tail and the segmental lining. When the shield reaches the geometric turning limit, the maximum angular deviation is expressed as

$$\sin \alpha_{\max} = \frac{L_2}{L_1} \tag{4}$$

For the investigated shield machine, $L_1 = 28.0$, and $L_2 = 0.47$ m; therefore,

$$\alpha_{\max} = \arcsin\left(\frac{L_2}{L_1}\right) = \arcsin\left(\frac{0.47}{28.0}\right) = 0.962^{\circ} \tag{5}$$

The segment outer diameter is $D_w = 13.6$ m, and the segment thickness is 0.55 m; thus, the inner diameter is $D_n = 12.5$ m, and the effective diameter is

$$D = \frac{D_w + D_n}{2} = \frac{13.6 + 12.5}{2} = 13.05 \text{ m} \tag{6}$$

Substituting D and $\alpha_{\max}$ into Equation (1) gives

$$\delta_{\max} = D \sin \alpha_{\max} = 13.05 \times \frac{0.47}{28.0} = 0.219 \text{ m} = 21.9 \text{ cm} \tag{7}$$

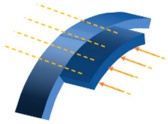
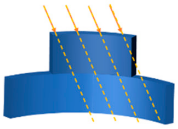
Therefore, the shield tail clearance enters the calculation directly through L_2, and 21.9 cm represents the project-specific geometric or kinematic upper limit rather than a structural damage threshold.

4.5. Establishment of Control Criteria for Shield Attitude Deflection

Finite element simulations of segment–bolt systems reveal the stress states during assembly. Under asymmetric loading, unclosed segment rings exhibit reduced structural safety, leading to critical damage at specific deflection angles. These angles correlate with allowable differential jack strokes to mitigate risks. Concurrently, bolt stresses gradually diminish during assembly, as validated by numerical simulations and field tests. Analysis confirms that bolt stresses remain below yield thresholds, ensuring structural integrity under STAT conditions. By integrating asymmetric and locally eccentric loading scenarios, this study quantifies bolt stress responses during segment failure initiation. Numerical simulations in Section 4.1 identify critical failure angles across segment positions, with detailed values provided in Table 3. These results demonstrate that bolt safety is preserved even under extreme asymmetric loads inherent to STAT operations.

In this study, the critical segment angle was defined as the first loading increment at which localized concrete damage appeared in the FE results based on the adopted elastoplastic damage model. It represents damage initiation rather than complete structural failure or a measured crack-width limit. Bolt safety was evaluated by comparing the calculated and measured stresses with the yield strength of 640 MPa. No additional safety factor or probabilistic uncertainty factor was applied; therefore, the reported thresholds should be interpreted as project-specific deterministic limits.

Table 3. Attitude control criteria of segment assembly.

Segment Deflection	Stress Diagram	Assembly Location	Assembly Sequence	Structure Deflection Angle	Shield Tail Jack Stroke Differential	Assembly Part	Assembly Sequence	
Radial deflection to the tunnel		Crown	First piece	0.60°	1.05 cm	Crown	First piece	
			Second piece	0.71°	1.25 cm			
			Third piece	0.60°	1.05 cm			
		Haunch	First piece	0.57°	1.00 cm		Second piece	
			Second piece	0.78°	1.37 cm			
			Third piece	0.79°	1.39 cm			
		Invert	First piece	0.64°	1.12 cm		Third piece	
			Second piece	0.71°	1.25 cm			
			Third piece	0.60°	1.05 cm			
Radial deflection to the outside of the tunnel		Crown	First piece	1.20°	2.13 cm	Haunch	First piece	
			Second piece	1.00°	1.76 cm			
			Third piece	0.58°	1.02 cm			
		Haunch	First piece	1.10°	1.93 cm		Second piece	
			Second piece	0.76°	1.37 cm			
			Third piece	0.58°	1.02 cm			
		Invert	First piece	0.58°	1.02 cm		Third piece	
			Second piece	0.76°	1.37 cm			
			Third piece	0.40°	0.70 cm			
Lateral deflection along the tunnel		Crown	First piece	1.40°	12.0 cm	Invert	First piece	
			Second piece	1.81°	15.5 cm			
			Third piece	1.38°	11.8 cm			
		Haunch	First piece	1.41°	12.1 cm		Second piece	
			Second piece	1.82°	15.6 cm			
			Third piece	1.37°	11.7 cm			
		Invert	First piece	1.39°	11.9 cm		Third piece	
			Second piece	1.89°	16.2 cm			
			Third piece	1.38°	11.8 cm			

Finite element simulations of segment assembly reveal position-dependent critical damage initiation angles. Within the deterministic FE simulations conducted for the investigated project, outward radial deflection produced the lowest damage initiation threshold among the considered loading modes. Specifically, damage initiation was first observed at a segment deflection angle of 0.40°, corresponding to a differential jack stroke of 0.70 cm. This result should be interpreted as a model-based deterministic threshold rather than a statistically bounded failure probability, because formal uncertainty analysis was not conducted in the present study. The 0.40° value was obtained from the most unfavorable configuration among the modeled one- to three-segment incomplete-ring stages. It is therefore regarded as a conservative early-stage control threshold for the investigated project, rather than a threshold validated for every subsequent assembly stage, including key-segment insertion and ring closure. Mechanically, outward radial deflection tends to reduce the effective contact restraint between adjacent segments, cushion layers, and waterstop rubber gaskets, thereby weakening the temporary clamping effect of incomplete segmental lining rings. Meanwhile, the eccentric jack thrust path increases local compression and bending effects near segment edges and joint regions, leading to earlier stress concentration and damage

initiation than inward radial or lateral deflection under the investigated conditions. For the investigated project, the segment inner radius is $R_1 = 6250$ mm, and the outer radius is $R_2 = 6800$ mm, based on the segment outer diameter of 13.6 m and thickness of 550 mm. The segment chord length is $L_4 = 4912.88$ mm, and the corresponding vertical geometric distance $L_3 = 1006.91$ mm, which was obtained from the project segment geometry, as defined in Figure 12. These geometric dimensions were subsequently used in Equations (2) and (3) to convert the critical deflection angles into differential jack strokes. Using Equations (2) and (3), the corresponding critical differential jack stroke was calculated. Collision analysis confirmed that outward-deflecting segments maintain safe clearance from the tunnel lining. This enables direct correlation between segment deflection angles and controlled jack stroke differentials, establishing angular-to-stroke conversion as a viable control strategy.

As shown in Table 3, the initial failure angle of the segment is 0.4°, corresponding to a differential jack stroke of 0.7 cm, while the maximum deflection failure angle of 1.82° corresponds to a stroke differential of 15.6 cm. However, based on the geometric turning relationship of the shield machine in actual engineering applications, the maximum allowable differential jack stroke does not exceed 21.9 cm. Notably, this upper threshold was not reached in the simulated failure angle scenarios, indicating that structural damage initiates before the kinematic limits of the shield are approached.

5. Discussion

The present study established an integrated attitude control framework for large-diameter shield tunneling under STAT conditions by combining numerical simulations, field tests, and engineering validation. Although the proposed criteria provide a practical reference for shield construction, several issues require further discussion.

The earlier damage initiation observed under outward radial deflection can be explained by the mechanical characteristics of incomplete segmental lining rings under STAT conditions. Unlike completed rings in conventional shield tunneling, incomplete segmental lining rings cannot provide full circumferential confinement during assembly. When outward radial deflection occurs, the segment tends to rotate away from the completed ring, reducing interface compression between the segment, cushion layer, and sealing gasket. This weakens the temporary clamping effect formed during segment assembly and amplifies the eccentric transfer of jack thrust. Consequently, local compression, bending deformation, and stress concentration develop more rapidly near the segment edges and bolt-joint regions. In contrast, inward radial deflection tends to push the segment toward the completed ring, which partially enhances contact restraint, while lateral deflection is more strongly affected by the interaction between adjacent segments and bolts. Therefore, outward radial deflection was identified as the most unfavorable loading mode in the deterministic simulations of the present case project. Nevertheless, because the thresholds were obtained from a project-specific FE model, they should not be regarded as general uncertainty-bounded criteria. Future studies should incorporate parametric sensitivity analysis, construction randomness, material variability, and additional field monitoring data to quantify the uncertainty range of the proposed control thresholds. The FE model considered only one- to three-segment assembly stages. The reduction in bolt loads from the two-segment to the three-segment configuration indicates increasing restraint within the modeled range but does not demonstrate that the clamping effect becomes saturated after the third segment. Key-segment insertion and ring closure involve different boundary conditions and require further full-sequence analysis.

First, compared with conventional shield tunneling, STAT introduces a unique loading mechanism in which jack thrust acts directly on incomplete segmental lining rings before

ring closure. Under such conditions, the load transfer mechanism between segments and bolts becomes more complex due to the absence of complete circumferential constraints. The numerical results indicate that asymmetric loading significantly affects stress redistribution and damage evolution within the segment–bolt system. In particular, radial outward deflection represents the most unfavorable loading condition, where structural damage initiates earlier than under other loading modes. This finding suggests that construction quality control should focus on preventing excessive outward displacement during assembly.

Second, the field measurements showed larger bolt stress responses than the finite element predictions. Installation prestress, construction tolerances, installation errors, and variations in embedded-component positions may have contributed to this difference. However, no direct preload measurements, tightening-torque records, or statistical error distributions were available. Therefore, the contribution of each factor and the absolute safety margin relative to the bolt yield strength cannot be quantified in the present study. Further evaluation requires instrumented bolt-tightening tests and repeated measurements from additional rings. This difference is mainly due to three key factors: (a) bolt prestressing induced by impact-drill installation procedures; (b) construction and assembly uncertainties, including assembly tolerances and installation errors; and (c) local variations in the positions of embedded components. These factors inevitably influence the actual stress distribution in the segment–bolt system. Therefore, although the proposed finite element model can effectively capture the overall mechanical behavior, introducing construction uncertainties into numerical simulations would further improve predictive accuracy.

Only Ring 1488 was monitored in the present field test; therefore, repeatability and inter-ring variability could not be statistically evaluated. Multi-ring monitoring is recommended in future studies.

Third, the proposed shield attitude control criteria were established based on a specific large-diameter shield project. Although the methodology itself is generally applicable, the threshold values obtained in this study may vary with project characteristics such as tunnel diameter, segment geometry, geological conditions, shield machine configuration, and construction parameters. Therefore, the direct application of the current criteria to other projects should be conducted cautiously, and calibration based on project-specific conditions is recommended.

The angle–stroke relationships adopted in this study are based on deterministic rigid-body geometry. In practice, ground variability, shield–soil interaction, hydraulic system response, assembly tolerances, and operational disturbances may alter the actual relationship. A complete uncertainty propagation analysis would require additional parameter distributions, repeated simulations, and multi-ring field measurements, which were unavailable in the present study. Therefore, the proposed values should be calibrated before application to other projects.

Finally, several limitations remain in the present study. The numerical simulations mainly considered static asymmetric loading conditions and simplified some complex construction interactions. Time-dependent effects, such as dynamic loading induced by machine vibration, cyclic loading during continuous tunneling, and long-term structural response, were not explicitly investigated. Future research should focus on developing more comprehensive numerical models incorporating bolt pretension, construction randomness, and soil–structure interaction effects. In addition, more field monitoring data from different engineering projects are required to further validate and optimize the proposed attitude control criteria. The omission of detailed thread geometry and the use of an idealized tie constraint may suppress local stress concentrations at the thread roots and relative slip at the bolt–insert interface. No dedicated sensitivity comparison with threaded or frictional-

contact models was performed. Therefore, the present conclusions are limited to the global bolt-shank response, while local thread failure requires further refined analysis.

In addition, although local mesh refinement and nonlinear convergence checks were adopted in the finite element simulations, a systematic mesh independence study using multiple mesh densities was not performed in the present work. Therefore, the predicted damage initiation angles and bolt stress responses should be interpreted as deterministic results based on the adopted modeling strategy. Future studies should further evaluate mesh sensitivity, contact parameter sensitivity, and numerical uncertainty to improve the reproducibility and generality of the proposed control criteria.

6. Conclusions

Under the innovative STAT mode, critical safety risks arise from asymmetric stress distribution in unclosed segment rings and excessive segment deflection. The novelty of this study lies in linking shield attitude control with the mechanical safety of incomplete segmental lining rings and bolts under STAT conditions. Unlike conventional attitude control methods that mainly rely on geometric deviation indicators, the proposed framework quantitatively couples segment damage thresholds, bolt stress safety, shield tail clearance, and jack stroke constraints. This enables the conversion of critical segment deflection angles into allowable differential jack strokes, providing a project-specific quantitative basis for attitude control during simultaneous propulsion and segment erection. The main conclusions are summarized as follows:

1. The critical failure angles of segments and bolt safety during assembly were investigated, and field measurements from Ring 1488 provided case-based support for the simulated bolt stress trends under the recorded construction conditions. The project-specific geometric or kinematic upper limit of the differential jack stroke was determined to be 21.9 cm, while all simulated conditions remained below this value. The differential jack strokes corresponding to the damage initiation conditions listed in Table 3 were all below 21.9 cm, suggesting that, under the investigated conditions, segment damage may initiate before the shield approaches its kinematic stroke limit. The obtained failure angles can provide practical guidance for engineering construction.
2. Shield attitude deviations in actual engineering are multidimensional and lead to complex asymmetric loading conditions. Numerical simulations under a 2° deflection condition indicated that bolt stresses remained within safe limits, demonstrating adequate structural safety.
3. The measured bolt stress responses exceeded the finite element predictions. Because the installation preload, tightening torque, and statistical uncertainty were not measured, the discrepancy could not be quantitatively partitioned, and the field results should not be interpreted as an absolute assessment of the bolt yield-strength margin.
4. For the modeled early-stage incomplete-ring configurations, the minimum radial damage initiation angle was 0.4° (corresponding to 0.7 cm), while the minimum lateral damage initiation angle was 1.37° (corresponding to 11.7 cm). These values should be regarded as conservative, project-specific control references pending validation over the complete ring-assembly sequence.
5. Based on the interaction between segment failure mechanisms and shield machine operating constraints, corresponding attitude control criteria were established, providing practical guidance for optimizing assembly procedures and improving construction efficiency.
6. The conclusions should be interpreted within the scope of the investigated project. Bolt pretension was not explicitly included in the numerical model, the proposed

thresholds are project-specific, and no formal uncertainty analysis was conducted. Further validation is therefore required before applying the criteria to other projects.

Author Contributions: Z.Z.: Conceptualization, data curation, formal analysis, and funding acquisition. J.Z.: Conceptualization, methodology, data curation, formal analysis, visualization, validation, and writing—original draft. F.P.: Funding acquisition and writing—review and editing. J.L.: Visualization and writing—review and editing. H.H.: Conceptualization, methodology, investigation, data curation, formal analysis, and funding acquisition. Y.Q.: Funding acquisition and writing—review and editing. X.K.: Funding acquisition and writing—review and editing. C.W.: Writing—review and editing. All authors have read and agreed to the published version of the manuscript.

Funding: This work was supported by the Shanghai "Science and Technology Innovation Action Plan" Outstanding Academic/Technical Leaders Program (Project No. 23XD1431200). This work was supported by Shanghai "Science and Technology Innovation Action Plan" Social Development Science and Technology Research Project (Project No. 21DZ1201100).

Data Availability Statement: The original contributions presented in this study are included in the article. Further inquiries can be directed to the corresponding author.

Conflicts of Interest: Authors Yan Qiu and Xiaoyon Kou were employed by the company Shanghai Tunnel Engineering Co., Ltd. The remaining authors declare that the research was conducted in the absence of any commercial or financial relationships that could be construed as a potential conflict of interest.

References

1. Tan, Z.S.; Li, Z.L.; Tang, W.; Chen, X.Y.; Duan, J.M. Research on stress characteristics of segment structure during the construction of the large-diameter shield tunnel and cross-passage. *Symmetry* **2020**, *12*, 1246. [CrossRef]
2. Dai, H.B.; Ji, Y.G. STATistical analysis of chinese large-diameter shield tunnel and STATe-of-art and prospective of comprehensive technologies. *Tunn. Constr.* **2022**, *42*, 757–783. (In Chinese)
3. Zhu, M.; Chen, X.S.; Wang, X.T. Analysis and thinking on structural performance evolution of shield tunnel lining. *Eng. Mech.* **2022**, *39*, 33–50. (In Chinese)
4. Guo, L.; Huang, Z.; Zhang, D.; Pitilakis, K.; Lu, D.; Yao, Z. Seismic response of soil-shield tunnel system considering spatial variability of multivariate soil properties via random field theory. *Tunn. Undergr. Space Technol.* **2026**, *174*, 107726. [CrossRef]
5. Kamiya, S.; Nishi, A. Shield Jacking and Assembly Simultaneous Construction Method. Japan Patent No. JP2005146762A, 9 June 2005.
6. Zhu, Y.T.; Zhu, Y.F.; Chen, E.J.; Zhai, Y.X.; Min, R.; Tang, B.; Huang, X. Synchronous shield tunnelling technology combining advancement and segment fabrication: Principle, verification and application. *Undergr. Space* **2023**, *13*, 23–47. [CrossRef]
7. Zhu, Y.T.; Min, R.; Qin, Y.; Wu, W.F.; Yuan, P.; Zhai, Y.X.; Zhu, Y.F. Development and application of a model test platform of synchronous technology combining shield tunneling with segment assembling. *J. Shanghai Jiao Tong Univ.* **2022**, *56*, 897–907. (In Chinese)
8. Zheng, Y.G.; Wang, P.X.; Fan, Y.L.; Zhou, K. Analysis of synchronous pushing construction of tunnel boring machine. *Constr. Mach.* **2023**, 149–153. (In Chinese)
9. Gong, C.J.; Ding, W.Q.; Mosalam, K.M.; Günay, S.; Soga, K. Comparison of the structural behavior of reinforced concrete and steel fiber reinforced concrete tunnel segmental joints. *Tunn. Undergr. Space Technol.* **2017**, *68*, 38–57. [CrossRef]
10. Jin, H.; Yuan, D.J.; Wang, E.Z.; Jin, D.L.; Shen, X. Experimental investigation on shield-soil interaction during shield posture adjustment in soft ground. *Tunn. Undergr. Space Technol.* **2025**, *158*, 106386. [CrossRef]
11. Gil Lorenzo, S. The role of temporary spear bolts in gasketed longitudinal joints of concrete segmental linings. *Tunn. Undergr. Space Technol.* **2020**, *105*, 103576. [CrossRef]
12. Shi, P.X.; Li, P. Mechanism of soft ground tunnel defect generation and functional degradation. *Tunn. Undergr. Space Technol.* **2015**, *50*, 334–344. [CrossRef]
13. Zheng, G.; Cui, T.; Cheng, X.S.; Diao, Y.; Zhang, T.Q.; Sun, J.B.; Ge, L.B. Study of the collapse mechanism of shield tunnels due to the failure of segments in sandy ground. *Eng. Fail. Anal.* **2017**, *79*, 464–490. [CrossRef]
14. Ding, Z.; Zhang, M.B.; Zhang, X.; Wei, X.J. Theoretical analysis on the deformation of existing tunnel caused by under-crossing of large-diameter slurry shield considering construction factors. *Tunn. Undergr. Space Technol.* **2023**, *133*, 104913. [CrossRef]
15. Shi, C.H.; Wang, Z.X.; Gong, C.J.; Liu, J.W.; Peng, Z.; Cao, C.Y. Prediction of the additional structural response of segmental tunnel linings induced by asymmetric jack thrusts. *Tunn. Undergr. Space Technol.* **2022**, *124*, 104471. [CrossRef]

16. Wang, H.; Gao, X.; Li, P.; Jia, Z. Analysis of compressive bending capacity in bolted circumferential joint of shield tunnels. *J. Beijing Jiaotong Univ.* **2022**, *46*, 114–122.
17. Long, W.; Chen, W.J.; Huang, C.F.; Li, D.Y.; Su, D. Study on transverse deformation characteristics of a shield tunnel under earth pressure by refined finite element analyses. *Symmetry* **2022**, *14*, 2030. [CrossRef]
18. Cui, Q.L.; Li, J.; Gao, B.Y.; Xiong, X.Y. Mechanical Properties of Three-inclined Bolts in Longitudinal Joint of Large-diameter Shield Tunnel Segment. *Mod. Tunn. Technol.* **2022**, *59*, 63–71. (In Chinese)
19. Li, Z.; Soga, K.; Wang, F.; Wright, P.; Tsuno, K. Behaviour of cast-iron tunnel segmental joint from the 3D FE analyses and development of a new bolt-spring model. *Tunn. Undergr. Space Technol.* **2014**, *41*, 176–192. [CrossRef]
20. Chen, J.S.; Mo, H.H. Numerical study on crack problems in segments of shield tunnel using finite element method. *Tunn. Undergr. Space Technol.* **2009**, *24*, 91–102. [CrossRef]
21. Cavalaro, S.H.P.; Blom, C.B.M.; Walraven, J.C.; Aguado, A. Structural analysis of contact deficiencies in segmented lining. *Tunn. Undergr. Space Technol.* **2011**, *26*, 734–749. [CrossRef]
22. Ge, S.P.; Xie, D.W.; Ding, W.Q.; Ouyang, W.B. Simplified numerical simulation method for segment joints of shield tunnels. *Chin. J. Geotech. Eng.* **2013**, *35*, 1600–1605. (In Chinese)
23. Arnau, O.; Molins, C. Theoretical and numerical analysis of the three-dimensional response of segmental tunnel linings subjected to localized loads. *Tunn. Undergr. Space Technol.* **2015**, *49*, 384–399. [CrossRef]
24. Fu, S.S. Analysis of the Influence of Shield Construction on the Force of Segment Structure. Master's Thesis, Beijing Jiaotong University, Beijing, China, 2010. (In Chinese)
25. Dai, Z.Y.; Li, P.N.; Zhu, M.Q.; Zhu, H.H.; Liu, J.; Zhai, Y.X.; Fan, J. Dynamic prediction for attitude and position of shield machine in tunneling: A hybrid deep learning method considering dual attention. *Adv. Eng. Inform.* **2023**, *57*, 102032. [CrossRef]
26. Liu, X.; Yang, Z.H.; Men, Y.Q. Temporal variation laws of longitudinal stress on cross section of shield tunnels. *Chin. J. Geotech. Eng.* **2021**, *43*, 188–193. (In Chinese)
27. Hu, M.; Wu, B.J.; Zhou, W.B.; Wu, H.M.; Li, G.; Lu, J.; Yu, G.; Qin, Y. Self-driving shield: Intelligent systems, methodologies, and practice. *Autom. Constr.* **2022**, *139*, 104326. [CrossRef]
28. Liu, S.J.; Shi, L.K.; Wei, Y.J.; Wang, H.W.; Du, J.K.; Wang, J.; Yu, Y.X.; Zhu, L. Study on thrust vector control method for shield synchronous propulsion and assembly based on thrust uniformity. *Mod. Tunn. Technol.* **2024**, *61*, 10–20. (In Chinese)
29. Yuan, M.Z.; Zhang, J.L.; Cao, W.B.; Liu, X. Geometric Analysis of the Erection Quality of the Single-ring of Segments with New Connectors. *Mod. Tunn. Technol.* **2018**, *S2*, 57–65. (In Chinese)
30. Xiao, H.H.; Yang, W.K.; Hu, J.; Zhang, Y.P.; Jing, L.J.; Chen, Z.Y. Significance and methodology: Preprocessing the big data for machine learning on TBM performance. *Undergr. Space* **2022**, *7*, 680–701. [CrossRef]
31. Yang, M.; Ji, Z.Y.; Zhang, L.; Zhang, A.W.; Xia, Y.M. A hybrid comprehensive performance evaluation approach of cutter holder for tunnel boring machine. *Adv. Eng. Inform.* **2022**, *52*, 101546. [CrossRef]
32. Zhou, S.Y.; Liu, S.L.; Kang, Y.L.; Cai, J.; Xie, H.M.; Zhang, Q. Physics-based machine learning method and the application to energy consumption prediction in tunneling construction. *Adv. Eng. Inform.* **2022**, *53*, 101642. [CrossRef]
33. Huang, L.C.; Huang, S.; Lai, Z.S.; Liang, Y. The effective flexural stiffness of segment joints in large-diameter tunnel under various loading conditions. *Struct. Concr.* **2020**, *21*, 2824–2835. [CrossRef]
34. Li, X.J.; Yan, Z.G.; Wang, Z.; Zhu, H.H. Experimental and analytical study on longitudinal joint opening of concrete segmental lining. *Tunn. Undergr. Space Technol.* **2015**, *46*, 52–63. [CrossRef]
35. Nan, J.J. Research on the construction challenges of reinforcing a large area of deep soft soil layer with circular underground continuous wall anchor foundation. *Highway* **2023**, *68*, 145–150. (In Chinese)
36. Wang, Z.Y.; Yang, H.; Lin, G.; Lian, Z.Z.; Yu, B. Analysis of the impact of connecting bolts on the vibration response of shield tunnels. *Mod. Tunn. Technol.* **2024**, *61*, 172–179. (In Chinese)

Disclaimer/Publisher's Note: The statements, opinions and data contained in all publications are solely those of the individual author(s) and contributor(s) and not of MDPI and/or the editor(s). MDPI and/or the editor(s) disclaim responsibility for any injury to people or property resulting from any ideas, methods, instructions or products referred to in the content.